Helsinki University of Technology
Department of Electrical and Communications Engineering
Metrology Research Institute
Espoo 2003

MEASUREMENT OF EPITHELIAL ELECTRICAL PASSIVE PARAMETERS AND ITS APPLICATION TO STUDY GASTRIC DEFENCE AGAINST ACID AND ULCEROGENIC AGENTS

Harri Mustonen

Dissertation for the degree of Doctor of Science in Technology to be presented with due permission of the Department of Electrical and Communications Engineering for public examination and debate in Auditorium S5 at Helsinki University of Technology (Espoo, Finland) on the 28th of November, 2003, at 12 noon.

Helsinki University Central Hospital
Department of Surgery
Helsinki, Finland

Supervised by:
Professor of Surgery, M.D., Eero Kivilaakso
Department of Surgery
Helsinki University Central Hospital
Helsinki, Finland

Reviewed by:
Professor of Physiology, M.D., Gunnar Flemström,
Department of Physiology
University of Uppsala
Uppsala, Sweden

And

Docent, Ph.D., Ove Eriksson
Institute of Biomedicine
University of Helsinki
Helsinki, Finland

Opponent:
Professor, Ph.D., Juha Voipio
Department of Biosciences
University of Helsinki
Helsinki, Finland

ISBN 951-22-6798-5 (paperback)
ISBN 951-22-6794-2 (PDF)

Yliopistopaino
Helsinki 2003

To my family

TABLE OF CONTENTS

ABSTRACT

The aim of this study was to develop a reliable method for measuring epithelial membrane and shunt resistances. This was accomplished by improving the intraepithelial two dimensional cable analysis by using multiple electrodes simultaneously and by sequentially applying the intraepithelial current through different electrodes thus taking advantage of their spatial relationship. The improvement achieved with this novel method is its excellent temporal resolution; changes in the membrane and shunt pathway resistances can be typically measured in 9-20 seconds. The actual measurement time depends on the target tissue, number of electrodes, electrode noise and distance configuration.

This technique was applied to investigate the effects of luminal acid on membrane resistances of *Necturus* gastric (antral) mucosa. The main finding was that luminal acid closes sodium selective, amiloride blockable channels on the apical cell membrane probably by protonating 1-2 amino acid residues of the channel molecule itself. These findings suggest that the epithelium can generate a protective barrier against the luminal acidic offence by closing its apical cell membrane channels. Besides direct protection against H^+ influx, another possible advantage gained by closure of the Na^+-selective channels in the apical cell membrane is the maintenance of a sufficient transmembrane Na^+ gradient for Na^+-dependent acid equivalent transport processes across the basolateral cell membrane.

The method was also used to elucidate the effects of luminal ethanol on the epithelial membrane resistances of *Necturus* gastric mucosa. Surprisingly, the first effects were seen on the basolateral cell membrane, not on the apical cell membrane or on the shunt pathway, as would have been expected. With ion substitution and channel blocker experiments, it was deduced that potassium selective channels on the basolateral cell membrane were opened by luminal ethanol exposure. This opening of potassium channels decreased cell volume. The present data indicate that opening of basolateral K^+ channels with resultant epithelial cell shrinkage are among the earliest functional perturbations that might precede and underlie ethanol induced gastric mucosal injury. The subsequent opening of apical Na^+ selective channels with consequent increase in intracellular Na^+ load after more prolonged ethanol exposure suggests further functional deterioration of the epithelium. On the other hand, the profound changes in intraepithelial resistances provoked by stronger ethanol insult (i.e. collapse of R_a, decrease in R_s and closing of the gap-junctions as judged from the increased R_x) are more compatible with a structural damage of the epithelium and probably reflect emerging disruption of the surface epithelium.

LIST OF ORIGINAL PUBLICATIONS

This thesis is based on the following original publications, referred to in the text by Roman numerals:

I Kiviluoto T, Mustonen H, Kivilaakso E. Effect of Barrier-Breaking Agents on Intracellular pH and Epithelial Membrane Resistances: Studies in Isolated *Necturus* Antral Mucosa Exposed to Luminal Acid. Gastroenterology 1989; 96:1410-1418.

II Mustonen H. Improved Intraepithelial Two-Dimensional Cable Analysis with Application to *Necturus* Gastric Antral Mucosa. Pflügers Arch 1998; 436:646-652.

III Mustonen H, Kivilaakso E. Luminal Acid Increases Apical Cell Membrane Resistance in Isolated *Necturus* Antral Mucosa. Gastroenterology 1997;113:875-883.

IV Mustonen H, Kivilaakso E.Effect of Luminal Ethanol on Epithelial Resistances and Cell Volume in Isolated *Necturus* Gastric Mucosa. Dig.Dis.Sci 2003;48:2037-2004

AUTHOR'S CONTRIBUTION

The results presented in this thesis are a result of collaboration within the research group.

Publication I: The author has partly constructed the measurement equipment and designed a new perfusion chamber. He has also performed a few experiments and done most of the data analysis and mathematical calculations. He has also partly prepared the manuscript for publication.

Publication II: The author has done virtually everything by himself. He has constructed and partly designed the measurement equipment. He has designed and written the measurement and analysing software. He has also done all the mathematical calculations, simulations and writing. He has also performed the experiments, but has received technical assistance in that respect. He has also prepared the manuscript for publication.

Publication III: The author has used the equipment form publication II. He has also done most of the experiments, but has received technical assistance in that respect. Technical staff has performed some of the experiment series. The author has done all the data analysis and mathematical calculations. He has also done most of the writing and prepared the manuscript for publication.

Publication IV: The author has used the equipment from publication II. He has also done most of the experiments, but has received technical assistance in that respect. Technical staff has performed some of the experiment series. The author has done all the data analysis and mathematical calculations. He has also done most of the writing and prepared the manuscript for publication.

ABBREVIATIONS

2D	Two dimensional
β_p	Fitted parameters
Δ	Deflection
γ	Activity coefficient
λ	Space constant of the epithelium
ρ	Internal specific resistivity
A	Constant
a	Activity of an ion
a	Apical
AE1-3	Anionic exchanger 1-3
AF-6	the ras-binding protein acute lymphocytic leukaemia fusion-6
Ag-AgCl	Silver-Silver chloride
$a_{Na}^{\ i}$	Intracellular Sodium activity
APKC	Atypical protein kinase C
ASA	Acetylsalicylic acid
ASIP	atypical PKC isotype-specific interacting protein
ATP	Adenosine triphosphate
ATPase	Adenosine triphosphatase
a_{VDR}	Voltage divider ratio
C	Concentration of the ion, Capacitance
C_a	Apical cell membrane capacitance
C_b	Basolateral cell membrane capacitance
C_{bl}	basolateral to lateral intercellular space membrane capacitance
CO_2	Carbon dioxide
DIDS	4,4'-Diisthiocyanatostilbene-2,2'-disulphonate
E	Equilibrium potential, Electromotive force
EGF	Epidermal growth factor
ETOH	Ethanol
E_{TMA}	TMA activity signal from the electrode

F	Faradays constant
Eion	Electrochemical equilibrium potential for an ion
FAK	Focal adhesion kinase
h	Thickness of the epithelium
HCO_3^-	Bicarbonate
HCl	Hydrochloric acid
i_0	Applied current from the current passing electrode
i	Inside the membrane bound region
I_s	Current carried by ion S
JAM	Junction adhesion protein
K_0, J_0	Modified Bessel functions of second kind and zero order
K_1	Modified Bessel function of the second kind and first order
KCl	Potassium chloride
kD	Kilodalton
LIS	Lateral intercellular space
MDCK	Madin-Darby canine kidney
MES	2-[N-Morpholino] ethane-sulfonic acid
NaCl	Natriumchloride
NBC	Natrium bicarbonate cotransporter
NH_4^+	Ammonium ion
NHE1-4	Natrium proton exchangers 1-4
NMDG	N-Methyl-D-Glucamine
NMR	Nuclear magnetic resonance
NSAIDS	Nonsteroidal anti-inflammatory drugs
o	Outside of the membrane bound region
pH_i	Intracellular pH
P_S	Permeability through the membrane for an ion S
PKA	Protein kinase A
PKC	Protein kinase C
R	Common gas constant, Resistance
r	Distance from the current source
R_a	Apical cell membrane resistance

R_a/R_b	Ratio of apical to basolateral cell membrane resistances
R_b	Basolateral cell membrane resistance
R_{bl}	Basolateral cell membrane resistance to intercellular space
R_j	Tight junction resistance
R_{lis}	Lateral intercellular space resistance
R_m	Cell resistance to the bath solutions
R_m^{err}	Confounding error term of R_m
R_s	Shunt pathway resistance
R_{series}	Submucosal resistance
SEM	Standard error of the mean
T	Absolute temperature
t	Time
TGFα	Transforming growth factor α
TMA	Tetramethylammonium
V	Potential
V_{cm}	Apical cell membrane potential
V_{sm}	Transmucosal potential, mucosa as a reference
V_{ms}	Transmucosal potential, serosa as a reference
V_{cb}	Basolateral cell membrane potential
$V(x)$	Potential at the distance x
VAMP	Vesicle associated membrane protein
VAP-33	Vesicle associated membrane protein (VAMP) associated protein
z	Valence of an ion
ZAK	ZO associated kinase
ZO1,ZO2,ZO3	Zonula occludens-1, -2. -3
ZONAB	The transcription regulator ZO-1-associated nucleic acid binding protein
z_S	Valence for ion S
X	Derivative matrix

1. INTRODUCTION

Gastric and duodenal epithelia are the only epithelia, which have to withstand very large pH gradients. The acidity of gastric juice is of order pH 1-2, whereas the normal extra cellular (blood) pH is 7.4 and intracellular pH 7.2. The acid secreting parietal cells in the stomach can generate 150 mM concentration of protons in their primary secretion in gastric glands (Lloyd, Debas 1994) as compared to 63 nM encountered intracellularly, i.e. there is over a million fold gradient of protons across a single cell membrane approximately 6 nm thick. The breakdown of the defence system depends on multiple factors such as shortage of blood supply (large haemorrhage) or ulcerogenic agents, such as ethanol, aspirin (and other NSAIDs) and bile acids.

Approximately 10% of the western population suffers from gastric or duodenal ulcer during some period of their lives (Monson, MacMahon 1969). In Finland alone 10 000 sick leaves are caused annually by peptic ulcer disease and yearly over 300 Finns die of complications of ulcer disease, mainly due to bleedings and perforations. The incidence of peptic ulcer disease is decreasing, but the incidence of complications, such as perforations and bleeding is not and the overall mortality has doubled since early 1980's. Peptic ulcer disease is a very common disease and therefore its economical impact is remarkable.

The aim of this study is to develop and further refine experimental methods to measure different membrane resistances in gastric epithelia and to use these methods to elucidate the potential mechanisms of gastric defence against luminal acid and ulcerogenic agents. This study focuses on the gastric antrum, which is the distal part of the stomach (Fig 1.1). This study is a part of a research program on gastric defence and repair mechanisms performed at the Department of Surgery, University of Helsinki.

In an epithelium the apical cell membrane faces the lumen and the basolateral cell membrane faces the blood side of the cell. Between the cells there exits a paracellular pathway. The main resistive components of an epithelium are apical cell membrane resistance, basolateral cell membrane resistance and the shunt pathway resistance. These intraepithelial resistances have been usually measured by selectively changing one membrane resistance either with ion channel

inhibitors or by rapidly changing the ionic concentrations of perfusion solutions. Intracellular and transepithelial voltage response caused by a transepithelial current pulse are measured before and after cell membrane resistance change. Thereafter the resistances have been resolved from the changes made by the inhibitors or by the ion substitution using simple arithmetics. This approach requires that the inhibitor or the ion substitution affect only the apical or the basolateral cell membrane, respectively, although this is not always the case. It has been found with a sophisticated impedance analysis technique that barium, which is commonly used as a potassium channel blocker, also has an effect on transepithelial pathway in the Necturus gall bladder (Kottra, Frömter 1990a). We have observed that amiloride, which is used as an inhibitor of epithelial sodium selective channels, does not have this effect in acidic (pH 3.0) solutions (I). Amiloride also affects the Na^+/H^+ antiport thereby influencing intracellular pH balance, which also might perturb the results. The use of ion substitutions has also its limitations. For example, if the basolateral cell membrane has voltage dependent ion channels, a change in apical cell membrane potential due to an ion substitution on the apical side induces a change in basolateral cell membrane potential, thereby affecting voltage dependent ion channels and the basolateral cell membrane potential and resistance. It is evident that a method to measure epithelial membrane resistances, which would not rely on inhibitors or ion substitutions, would be preferable.

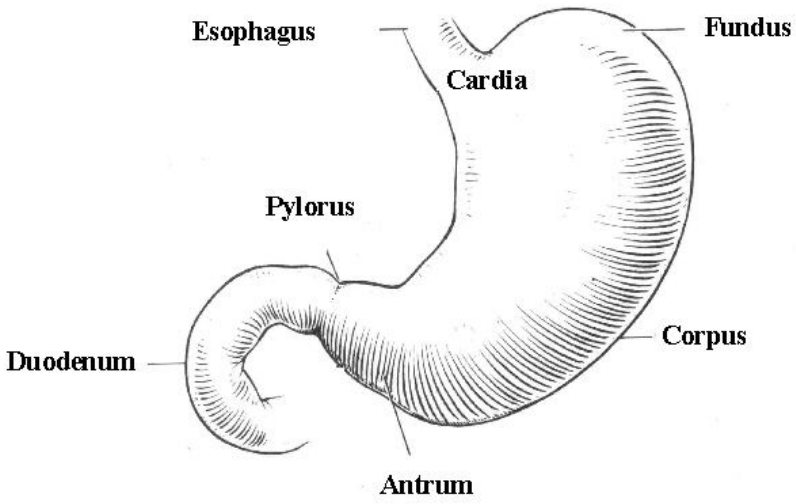

Fig 1.1 Structure of stomach. Modified from (Ito 1987)

The coupling of epithelial cells by gap junctions can be utilized in current spread experiments known as two dimensional intraepithelial cable analysis. Usually in this method two electrodes are used, one for passing current and the other for measuring voltage responses at several different distances from the current passing electrode. I have here developed a temporally superior method by using several microelectrodes simultaneously and by conducting the measurement current sequentially through different electrodes. I have also mathematically solved optimal distance configurations for the microelectrodes in order to obtain more reliable results.

This newly developed cable analysis method was applied to examine the effect of luminal acid on cell membrane resistances. The gastric mucosa must have efficient protective mechanisms to maintain physiological intracellular pH. It has been previously shown that the ratio of apical cell membrane resistance to basolateral cell membrane resistance (R_a/R_b) is increased due to luminal acid (Kivilaakso, Kiviluoto 1988; Rutten et al. 1989; Mustonen et al. 1992). If this increase is due to increase in the apical cell membrane resistance, it might serve as a protective mechanism against luminal acid. In order to further elucidate this increase in R_a/R_b, two-dimensional intraepithelial cable analysis, ion substitution and inhibitor experiments were performed in this work. Intracellular pH and sodium activity were also measured with ion selective microelectrodes during luminal acid exposure. It was found that luminal acid closes apical amiloride blockable sodium channels, probably by protonating a few amino acid residues in the channel protein. This closing was preceded with a small intracellular acidification and followed by a small decrease in intracellular sodium activity.

Luminal ethanol is a well-established barrier breaking agent in the gastric mucosa. Although many efforts have been made to find out the pathogenetic mechanisms of ethanol injury, the early pathophysiological events are still unknown Whether the early effects of ethanol are mediated through the fluidizing effect in the cell membrane phospholipids or by changes in membrane bound proteins is not known. The effect of luminal ethanol exposure is of course dependent on the ethanol concentration. Low concentrations of ethanol (0.25-4%) have been found to increase apical cell membrane resistance (Rutten, Moore 1991). Luminal exposure to 15% ethanol decreases the density of mitochondria and partially disrupts the apical cell membrane (Arakawa et al. 1992). Part of the effect of ethanol might be due to oxygen radicals

(Mutoh et al. 1990) and oxidative stress in mitochondria (Hirokawa et al. 1998). In another study, exposure to 12.5% ethanol produced widened and irregular intracellular spaces, while 20% and 40% ethanol disrupted the apical cell membrane (Dinoso et al. 1976). Although ethanol is often used in strongly hyperosmolar concentrations its influence in reducing cell volume is relatively weak. This is due to the high permeability of ethanol through the cell membranes. In rabbit gastric microsomes 0.5 M (ca 2.9% vol/vol) ethanol did not cause vesicle volume change (Ballard et al. 1988).

In this work I have used the two dimensional intraepithelial cable analysis, ion substitutions and inhibitor experiments to elucidate these mechanisms. I have also measured relative cell volume changes during luminal ethanol exposure. It was found that the first effects of ethanol on membrane resistances were the opening of basolateral potassium selective ion channels leading to cell volume shrinkage.

2. REVIEW OF THE LITERATURE

2.1 Structure of stomach

The stomach is a segment of the alimentary tract between the oesophagus and the duodenum (Fig 1.1). It produces a pulpy fluid called chyme from the chewed food by mixing and digesting it with gastric secretions. The chyme is passed to the duodenum. Nearly two litres of acidic (pH 1-2) gastric juice is secreted daily. In addition to acid it contains electrolytes, inactive precursors of pepsins called pepsinogens (which are activated by acid), intrinsic factor for vitamin B12 absorption, mucus, hormones (mainly gastrin, which increases gastric acid secretion and motility), enzymes (lipases, amylases and gelatinase) and water. The stomach absorbs very few substances. Some compounds such as aspirin and ethanol are absorbed in small amounts.

The barrier function of the stomach is formed by apical cell membranes of the surface epithelial cells, tight junctions between the cells, and mucus, bicarbonate and hormones secreted by the mucosa. For example, the apical cell membrane of the parietal cells have very low permeability to protons, which aids to prevent back diffusion of acids in to the cells (Hirst 1991). The tight junctions form a semi permeable barrier between the cells. Mucus adheres to epithelial surfaces and serves as a diffusion barrier against noxious substances and as a lubricant. Mucus consists mainly of mucins, salts and water. Mucins are a family of large heavily glycosylated proteins some of which are cell membrane bound. Mucins are secreted as large aggregates (1-10 Mdaltons). Glycosylation gives mucins large water holding capacity and makes them resistant to proteolysis. The carbohydrates in mucin molecules bind to bacteria thereby making it more difficult for bacteria to colonize (Forstner, Forstner 1994). Bicarbonate is secreted by mucous cells to the apical surface thereby increasing surface pH at the cell membrane (Kiviluoto et al. 1990; Flemström 1994). Prostaglandins are synthesized within the mucosa from arachidonic acid by cyclo-oxygenases. They stimulate mucus and bicarbonate secretion (Lloyd, Debas 1994) and increase mucosal blood flow (Tepperman, Jacobson 1994). Inhibition of cyclo-oxygenases by common nonsteroidal anti-inflammatory drugs (NSAIDs) is commonly associated with gastroduodenal ulcers. Two growth factors are associated with the maintenance of the barrier. Epidermal growth factor (EGF) is secreted in saliva and from duodenal glands, while transforming growth factor α (TGF-α) is produced by gastric epithelial cells. These growth

factors bind to the same EGF receptor and stimulate cell proliferation, enhance ulcer healing and inhibit acid production (Podolsky 1994). Trefoil peptides are secreted by goblet cells to the mucosal surface (Podolsky 1994). They play an important role in mucosal integrity and repair of lesions. In addition there is a strong immunological defence system in the gastrointestinal tract. The luminal content can be very hostile containing besides nutrients also micro-organisms and toxins. Certain compounds such as bile salts, ethanol and acetylsalicylic acid are able to disturb the gastric barrier and they are called barrier breakers.

The gastric wall has many distinctive layers: gastric mucosa, lamina propria, muscularis mucosae, submucosa, muscularis and serosa (Fig 2.1.1). Gastric mucosa consists of a single layer of epithelial cells, which are attached to the basement membrane (basal lamina) and form the gastric barrier between the gastric lumen and the mucosal tissue. The epithelium in the gastric mucosa forms also several glands, which secrete the gastric fluid. There are many cell types in the epithelium: mucous cells, parietal cells (secreting hydrochloric acid), chief cells (secreting pepsinogen), G cells (secreting the hormone gastrin) and D cells (secreting somatostatin). In addition there are enterochromaffin-like cells (secreting histamine in response to gastrin), goblet cells (secreting mucus) and undifferentiated cells. Mucous cells are mainly on the surface, whereas the other cells are mainly situated in the glands. Surface mucous cells are renewed approximately every 3-5 days. The mitotic activity is located in the pits and the cells migrate from there along the wall of the pit to the luminal surface of the stomach (Johnson, McCormack 1994). The cellular debris from the old dying cells is spread into the gastric lumen. Submucosa is a layer of connective tissue containing blood, lymphatic vessels and nerves. Muscularis consists of two thick layers of smooth muscle. Muscle fibres in the inner layer are circular, whereas those in the outer layer are longitudinal.

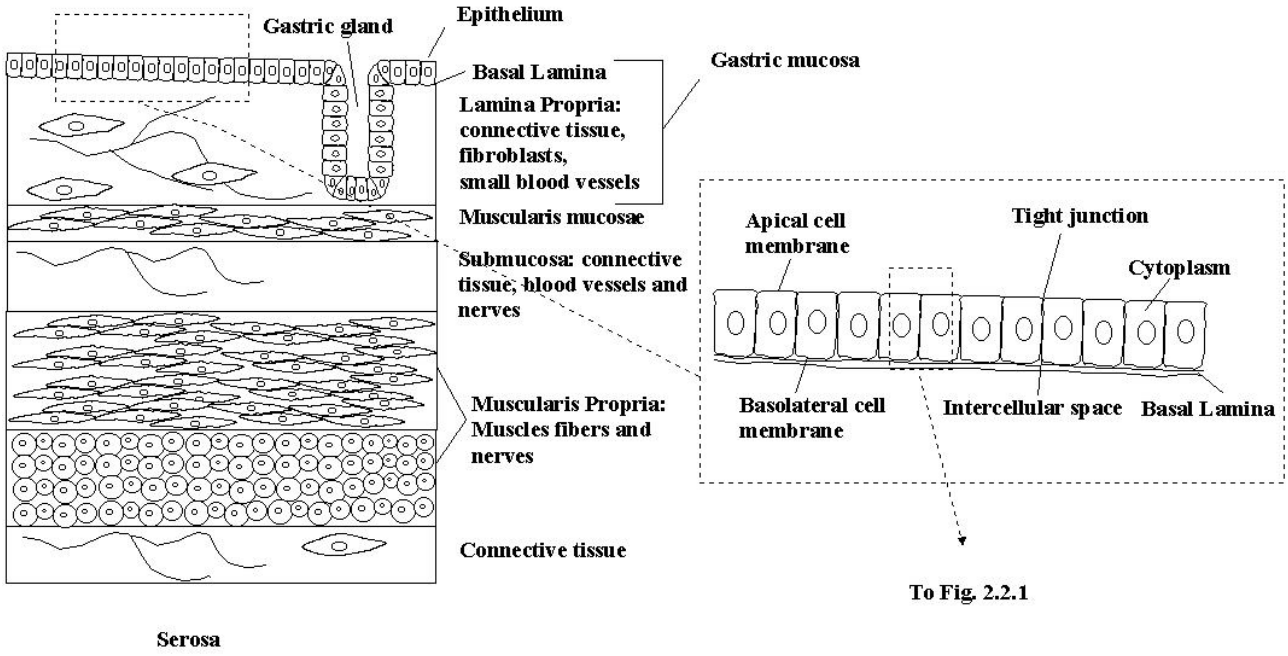

Fig 2.1.1 Simplified section of the stomach wall.

2.2 Cellular adhesion

In the epithelium of the gastric mucosa the cell-to-cell adhesion is mediated by cadherin family (Fig 2.2.1). In order to form cell adhesion, cadherin molecules dimerize laterally and interact in a calcium dependent manner with similar molecules of neighbouring cells (Vasioukhin, Fuchs 2001). They also cluster and bind to actin cytoskeleton via β- and α-catenin to form adherens junctions. Anchored cadherins act as traps for cadherins freely diffusing in the cell membrane (diffusion trap model) thus strengthening adhesion. At the beginning of cell contact there are discrete clusters of cadherin, β- and α-catenin in the cell contact area (discrete puncta) (Adams, Nelson 1998). Cadherins are also involved in desmosomes, where they connect the intracellular intermediate filament network of adjacent cells (Angst et al. 2001). The regulation of cell adhesion is complex, but at least Rho small GTPase family are involved (Kaibuchi et al. 1999). The adherens junctions may be involved in changes of lateral intercellular space resistance. Lateral intercellular space is the narrow space in between the cells and its width may be affected by attachment and detachment of adherens junctions.

Underneath the epithelium is a thin (40-120nm) sheet called basal lamina. The precise composition of basal lamina varies from tissue to tissue, but most basal laminae contain, at least, type IV collagen, perlecan (heparan sulphate proteoglycan), laminin and nidogen (Alberts et al. 2002). The cells above the basal lamina produce the above-mentioned proteins. Basal lamina is also important in wound healing, providing a scaffold for cell migration. Integrins are, in addition to dystroglycan (laminin binding receptor), the main protein family binding the cells to the extra cellular matrix. They link the extra-cellular matrix to the actin cytoskeleton at focal adhesions and to intermediate filaments at hemi-desmosomes. Actin filaments bind to integrins via talin, α-actinin, filamin or vinculin. Intermediate filaments bind to integrins via plectin. An integrin molecule is composed of two transmembrane subunits α and β. There are at least 24 different α subunits and 9 β subunits. Different integrins bind to different extracellular matrix proteins. Integrins activate various intracellular signalling pathways and often cooperate with conventional signalling receptors to regulate cell growth, migration, survival and proliferation (Juliano 2002). Integrin mediated signalling is probably involved in apoptosis (anoikis) of detached adherent cells. Tyrosine phosphorylation and activation of focal adhesion kinase (FAK) follows integrin-mediated adhesion and deactivation occurs right after the cells have detached. FAK plays a crucial role in cell motility and apoptosis (Juliano 2002). Integrins are also involved in cytoskeleton signalling via the Rho GTPases Rho, Rac and CDC42, although the exact mechanism is not known (Juliano 2002). On the other hand Rho GTPases are needed in focal adhesion formation.

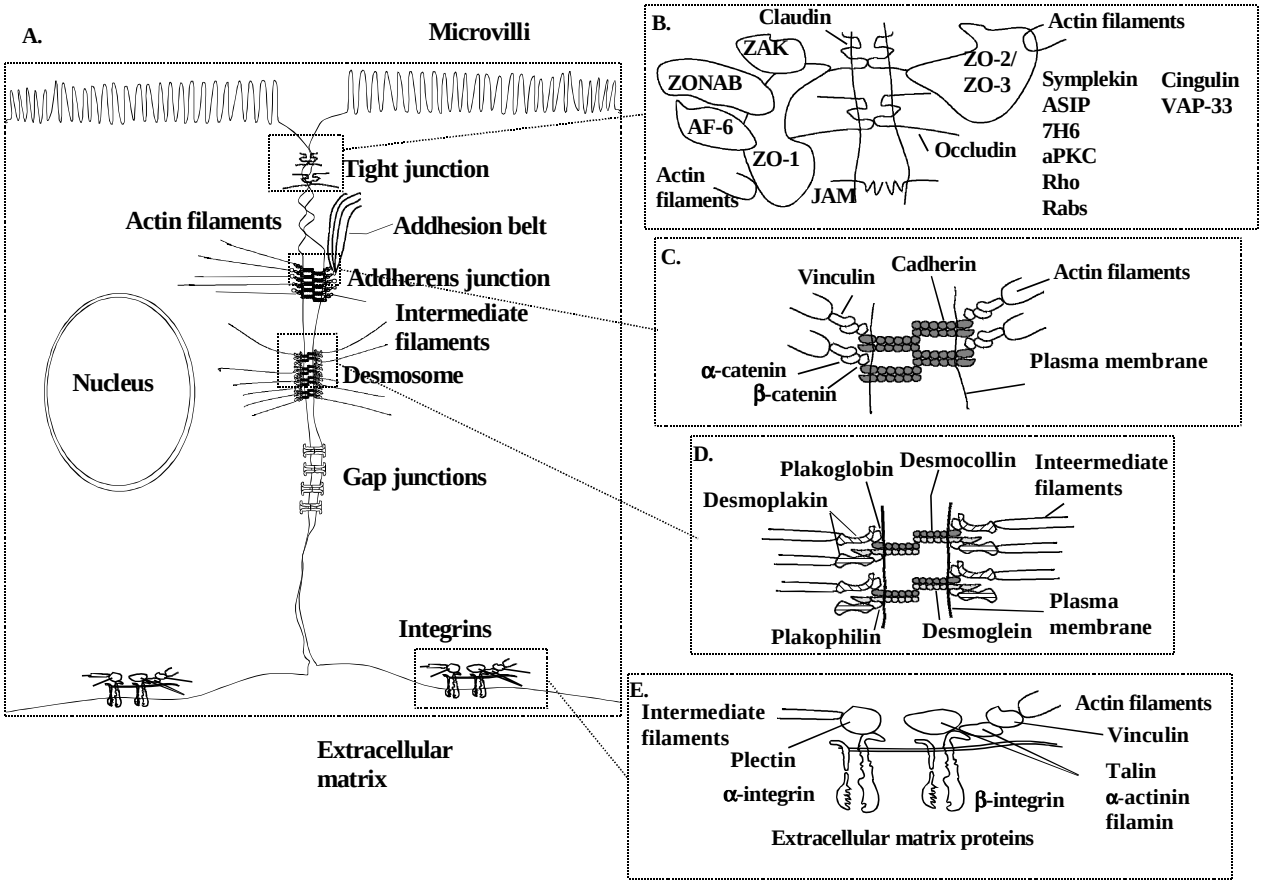

Fig 2.2.1 Location of junctional proteins in epithelia. A. A general view B The molecular components of tight junction. On the right side there is a list of proteins, which have been localized to tight junction, but their exact location and interaction partners have not been determined. C. Adherens junction D. Desmosome E. Cell to matrix adhesion.

2.3 Gap Junctions

Intercellular communication is mediated by gap junctions (Fig 2.3.1). These junctions are formed from a large family of connexin proteins. Connexin molecules oligomerize within the plasma membrane to form hemi-channels containing six connexin molecules. Two hemi-channels from neighbouring cells interact and form a pore between the cells. Small molecules (<2 kD) and ions are able to permeate through the pore (Stryer 1995). Over dozen connexin molecules have been identified. In excitable cells, gap junctions conduct the spread of electrical excitation from cell to cell. Increased intracellular free calcium activity is known to close the gap junctions (Reuss, Finn 1974). Increased intracellular free calcium activity is also related to cell death. Therefore the dying cell is isolated from the rest of the cell population. On the other hand the gap junctions can propagate slow calcium signals between the cells (Paul 1995). These junctions also allow the

applied current to a single cell to spread through the epithelium, which is utilized in the intraepithelial two-dimensional cable analysis.

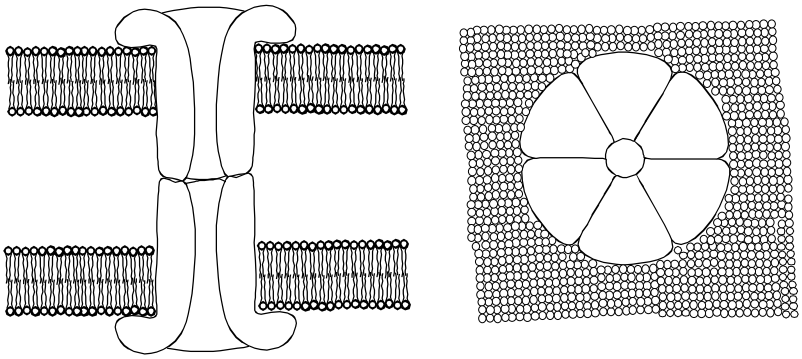

Fig 2.3.1 A schematic model of a gap-junction. Six connexin molecules oligomerize and form a hemi-channel. Two hemi-channels from the opposite cell membranes forms a gap junction

2.4 Tight junctions

Tight junctions (Fig 2.2.1) are complex protein structures, which form a belt-like band between the cells and seal the paracellular pathway. Tight junctions function as a barrier for solutes and water. In tight junction the adjacent cell membranes are in focal contacts to each other in several bands. In freeze fracture preparations tight junctions appears as a mesh-like continuous circumferential series of fibrils between the cells. Tight junction complex includes transmembrane proteins, such as occludins, claudins, junction adhesion molecule (JAM) and intracellular proteins, such as zonula occludens-proteins (ZO-1 - ZO-3), AF-6, and cingulin among others (Mitic et al. 2000). Transmembrane proteins form the actual tight junction and intracellular proteins act as linker and regulatory proteins. ZO proteins interact with occludins and claudins and connect them to actin cytoskeleton. This cross-linking is suggested to be involved in regulation of tight junctions (Tsukita et al. 1999). Occludin is one of the major constituents of tight junctions and they are heavily phosphorylated (Tsukita et al. 1999). Previously occludin was considered as the seal forming protein, but the recently discovered diverse claudin family is a more probable candidate for this function. Occludin can form only

short fibrils, whereas claudins usually form continuous fibrils (Mitic et al. 2000). Occludin, as well as claudins, has four membrane spanning domains, but occludin has longer carboxy and amino terminal domains than claudins. Distribution of the claudin family proteins is tissue specific and at the moment 20 different claudin proteins have been discovered. If extracellular calcium is lowered well below 0.1mM tight junctions are broken and tight junction components are retained in intracellular vesicles (Cereijido et al. 2000). If extracellular calcium is raised to 0.1mM, adherens junctions and tight junctions are formed. If the formation of adherens junctions is inhibited with E-cadherin antibody, also tight junctions are not formed (Cereijido et al. 2000). This suggests that the formation of adherens junctions is a prerequisite for tight junction formation.

From claudins 2-5 the claudin 3 and claudin 5 have been detected in the surface epithelial cells of the stomach. Surprisingly most of these claudins are located in the basolateral and lateral intercellular membranes, but not in tight junctions (Rahner et al. 2001). The reason for this paradox is not known, but either the claudins have also some role other than functioning as a tight junction protein or this spatial distribution provides a pool of claudins for regulatory purposes.

2.5 Cell membranes

All animal cells are enclosed by a cell membrane. These are lipid bilayers consisting mainly of phospholipids, many of which are built from a glycerol molecule esterified by a phosphate residue and by two fatty acids.

There are plenty of different phospholipids in the cell membranes including diphosphatidylglycerol, phosphatidylinositol, phosphatidylserine, phosphatidyletholamine, phosphatidylcholine and sphingomyelin (Stein 1987). Also cholesterol, a steroid, is an important constituent of many animal cell membranes. All these lipids have a hydrophilic portion, which strongly interacts with water (phosphate head group) and a hydrophobic portion, which repel water. In water phospholipids self-assemble into structures resembling cell membranes.

The distribution of phospholipids across the cell membrane is different. For example in a human red blood cell phosphatidylcholine and sphingomyelin are the major phospholipids at the outer face of the membrane bilayer, whereas phosphatidyletholamine and phosphatidylserine are located on the inside of the bilayer (Stein 1987). How, where and why this asymmetry is formed and maintained is still unclear. In endoplasmic reticulum, where some of the phospholipids are synthesized, the composition of phospholipid asymmetry is different from the cell membrane. In the Colgi apparatus the structure is still different, but probably more alike than in the endoplasmic reticulum. The pathway of phospholipids to the cell membranes goes through endoplasmic reticulum and Golgi apparatus. The composition of phospholipids is also different in apical and basolateral cell membranes (Sprong et al. 2001).

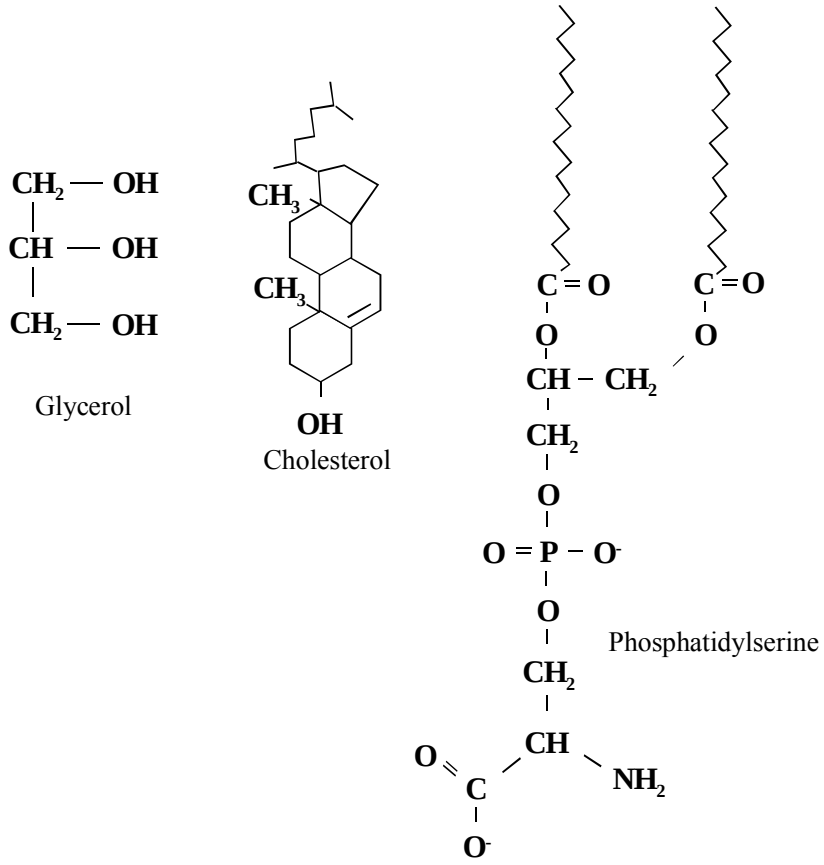

Fig 2.5.1 Glycerol, Cholestrol and, as an example, a phospholipid phosphatidylserine

Above 5-10 ^{0} C most of the phospholipids in the mammalian cell membranes are in fluid state. The fluidity of the membrane depends on the composition of phospholipids, on the ionic environment and on the temperature (Stein 1987). Membrane bound proteins increase the viscosity of the membrane bilayer. The thickness of phospholipid membranes is around 4-6 nm, depending on phospholipid composition (Sprong et al. 2001). The specific capacitance of these membranes is approximately 1 μF/cm^2. The resistance of pure phospholipid bilayers is high, approximately 10-1000 MΩ cm^2, and the physiologically relevant conductance across the bilayer is formed by ion channels (Hille 1984).

2.6 Cell membrane potential

The potential difference across the cell membrane depends on different ion concentrations on different sides of the membrane and on different permeability of ions through the membrane. Differences in ion concentrations on different sides of the membrane are maintained with active transportation of ions (Na^+/K^+ ATPase). Most biological membranes are more permeable to potassium than to sodium ions. If no net current flows through the membrane the cell membrane potential can be calculated from the equation [2.6.3]. Cell membrane potential causes relatively high electric field inside the membrane. If membrane potential is 70 mV and the thickness of the membrane is 7 nm, the electric field strength is 10^7 V/m. The equilibrium potential for an ion can be calculated from Nernst equation, which is deduced directly from the laws of thermodynamics:

$$E_{ion} = \frac{RT}{zF} \ln\left(\frac{a_o}{a_i}\right) \qquad [2.6.1]$$

, where E_{ion}=Electrochemical equilibrium potential for an ion, R=common gas constant, T=absolute temperature, z= valence of the ion, F=Faradays constant, a_o=ions activity outside of the membrane and a_i=ions activity inside the membrane bound region. If equilibrium potential of an ion is applied across a cell membrane, the electrical and chemical gradients of the ion repeal each other and the ion does not carry net current across the cell membrane. The activity of one ion type is proportional to their concentration $a=\gamma C$, where a= activity of an ion, γ=activity coefficient and C is the concentration of the ion. Activity coefficient depends on all the ions in

the solution and obeys Debye-Hückel theory (Amman 1986). Activity coefficients are near 1 in solutions with low ionic concentrations.

Ionic currents can be calculated, if the following simple assumptions are made: Independence of movement i.e. ions move without interacting with each other, electric field is constant inside the membrane and membrane is homogenous. The equation is called Goldman-Hodgkin-Katz current equation:

$$I_S = P_S z_S^2 \frac{EF^2}{RT} \frac{a_S^i - a_S^o \exp\left(\frac{-z_S FE}{RT}\right)}{1 - \exp\left(\frac{-z_S FE}{RT}\right)} \qquad [2.6.2]$$

, where P_S=permeability through the membrane for an ion S, E= membrane potential, z_S valence for ion S, R=common gas constant, T=absolute temperature, F=Faradays constant, a denotes activity, S a specific ion, superscripts i denotes inside and o outside of the membrane. This equation gives unlinear current voltage curves, when the ion activities are different in different sides of the membrane. From the current equation an equation for membrane reversal potential can be deduced. This Goldman-Hodgkin-Katz voltage equation gives the membrane potential at which no net current flows across the membrane and if only these three ions are involved:

$$E_{rev} = \frac{RT}{F} \ln\left(\frac{P_K a_K^o + P_{Na} a_{Na}^o + P_{Cl} a_{Cl}^i}{P_K a_K^i + P_{Na} a_{Na}^i + P_{Cl} a_{Cl}^o}\right) \qquad [2.6.3]$$

, where K, Na and Cl denotes for potassium, sodium and chloride, respectively.

2.7 Ion channels

As mentioned earlier the cell membranes are relatively impermeant to ions. Ion channels, pumps and transporters mediate ions and ion transport into and out of the cells. Ion channels are membrane bound proteins, which actually form an ion selective pore across the membrane with open-shut gating. The gating of ion channels may be intrinsic or regulated for example by ligand binding, changes of cell membrane voltage or by phosphorylation. With patch clamp techniques

developed by Neher and Sakmann (Neher, Sakmann 1976) single channel currents can be measured. In this technique a fire polished pipet is pushed against the cell membrane and a gigaohm seal is formed between the glass surface and the cell membrane. Single channel currents can be measured at pA range.

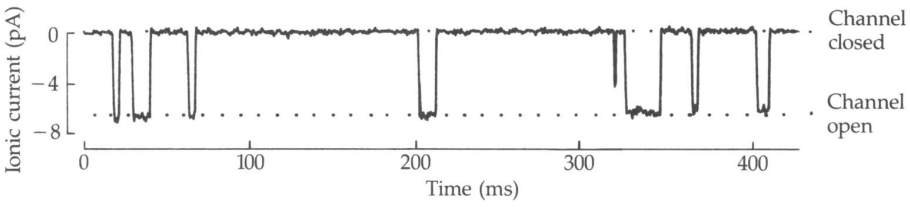

Fig 2.7.1 A single channel current. from (Hille 1984).

The open-shut frequency can be modulated with channel specific drugs or by normal cellular control mechanisms. Usually channels have only single conductance level, when open, but a few multistage channels have been found, which have two different conductance levels. It is believed that most of these channels actually have two pores (Hille 1984). Ion channels act as molecular sieves, the permeability cuts off at a definite size of the molecule. In addition there is a selectivity filter in the pore, which discriminates between different ion species. The selectivity filter is usually assumed to be located at the narrowest part of the pore and for example cation-selective channels usually have negatively charged residues near or at the selectivity filter. Ions in water are surrounded with water molecules. This ionic hydration shell is constantly changing and is usually partially torn off as the ions pass through an ion channel (Hille 1984).

As an example sodium selective amiloride inhibitable epithelial channel (ENaC) has very low potassium permeability (Pna/PK>10), but lithium permeates even better than sodium (Hille 1984). The channel is a hetero-oligomer formed form three different types of subunits: α β and γ. Single channel conductance of the ENaC is around 5pS. There is only slight voltage dependence in gating (Ashcroft 2000). The macroscopic current can be modulated for example with interactions with Nedd4-2 and Sgk1 (Kamynina, Staub 2002), which play a role in insertion and removal of the channel to and from the cell membrane. The macroscopic current of a cell membrane is the sum of ion fluxes through all the different types of channels located in the membrane.

In real channels the assumptions of Goldman-Hodgkin-Katz current equation are not strictly speaking valid. Instead, there is saturation, competition and blockage of channels, when the ionic activities are changed. Ions do not pass freely through the pore and they actually pause at various sites (Hille 1984).

2.8 Ion transporters

Eukaryotic cells have many ion transporters to maintain ionic and osmotic balance and to transport ions and nutrients across the cell membranes and epithelia. Animal cells have higher potassium than sodium concentration, while the situation is usually the reverse outside the cell. This concentration difference is maintained by the Na^+/K^+ ATPase, which pumps three sodium ions out and two potassium ions into the cell by hydrolysing one ATP molecule. This transport is slightly electrogenic, although its contribution to the cell membrane potential is usually low. The maintenance of a high sodium gradient across the cell membrane is essential, because this gradient is used for intracellular pH regulation, maintenance of low cytosolic calcium concentrations and transport of nutrients. Another important ATPase is the Ca^{2+} ATPase, which is also used in maintenance of low cytosolic calcium.

Active transport across the cell membrane can be powered by downhill transport of another solute or by ATP. In coupled transport either the solutes are simultaneously transported from one side of the membrane to the other by a symport or the solutes are transported to opposite directions by an antiport. Transporters are tightly coupled in order to function efficiently. In animal cells sodium usually has a large driving force across the cell membrane. This is utilised in many anti- and symporters. This is called secondary active transport, whereas ATP-driven transport is called primary active transport (Alberts et al. 2002).

Intracellular pH regulates many cellular processes including metabolism, cell-cell coupling and cell motility, and therefore intracellular pH is tightly regulated. Intracellular pH would be much lower without proton transport across the cell membranes. In *Necturus* gastric mucosa cell membrane potentials are around –40 mV. If protons were passively distributed across the cell

membranes, the intracellular pH would be 6.7, assuming extracellular pH 7.4. To maintain intracellular pH (pH_i) within normal range the cell uses plasma membrane proton pumps (H+-ATPase), ion transporters including Na^+/H^+ antiport, Na^+ dependent HCO_3^- transporter, Cl^-/HCO_3^- and Cl^-/OH^- exchangers and Na^+ HCO_3^-/Cl^- H^+ exchanger (Puceat 1999). Na^+/H^+ exchangers (NHE) have been identified in nearly all eukaryotic cells. They can be inhibited with amiloride and it's derivates (except NHE3). Six members of this exchanger have been cloned. NHE1 is a housekeeping exchanger and it has been found from almost all tissues. NHE1 has an ATP binding site, two Ca^{2+}-calmodulin binding sites and calcineurin homology protein binding site (Puceat 1999). Drop in intracellular ATP, increase in intracellular Ca^{2+} and hyperosmolarity increases NHE activity. In gastrointestinal tract NHE1-NHE4 are expressed (Puceat 1999). Growth hormones stimulate NHE exchangers, but the exact mechanism of this action is still under investigation.

Cells use Cl^-/HCO_3^- exchanger to survive from alkaline exposure. This anion exchanger family includes three types of exchangers AE1, AE2 and AE3. AE1 is expressed in spleen and erythrocytes. AE2 is expressed in most tissues and AE3 in stomach, kidney and brain. AE1 and AE3 are strongly inhibited by 4,4'-Diisthiocyanatostilbene-2,2'-disulphonate (DIDS) IC_{50}=1-10uM), whereas AE2 is poorly sensitive to this drug (IC_{50}=1mM) (Puceat 1999).

Na^+/HCO_3^- cotransporter (NBC) family is extremely diverse and they are found in most cell types. Stoichiometry changes from electroneutrality 1:1 to 1:3 (Na^+:HCO_3^-), NBSs being thus the most electrogenic transporters. NBCs are used both in influx and outflux of HCO_3^-. NBCs are inhibited with DIDS. NBC3 transporter has a PKA, several PKC and a tyrosine kinase binding site. NBCs are usually inhibited by PKA and PKC, but in the heart PKC activates the transporter (Puceat 1999).

Acid is secreted by parietal cells according to the current model: Potassium ions diffuse passively through an ion channel from the parietal cell into the lumen and are transported back to the parietal cell by H^+/K^+ ATPase, which simultaneously secretes protons into the lumen. Chloride ions diffuse passively through their ion channel into the lumen and thereby HCl is secreted. On the blood side of the parietal cell a Cl^-/ HCO_3^- exchanger balances for this loss of chloride by exchanging cytoplasmic bicarbonate (HCO_3^-) to chloride from the blood. In the

cytoplasm, H^+ and HCO_3^- are produced from carbonic acid (H_2CO_3), which is a product of water and carbon dioxide. This reaction catalysed by carbonic anhydrase, which is closely associated with the secretory membrane. (Sachs 1994).

2.9 Electrical models of epithelia

The electrical modelling of an epithelium is based on the knowledge of cell membrane properties and epithelial morphology. In figure 2.9.1 is a simple model for a cell membrane taking three most relevant ions into account. The voltage sources can be calculated from the Nernst equation.

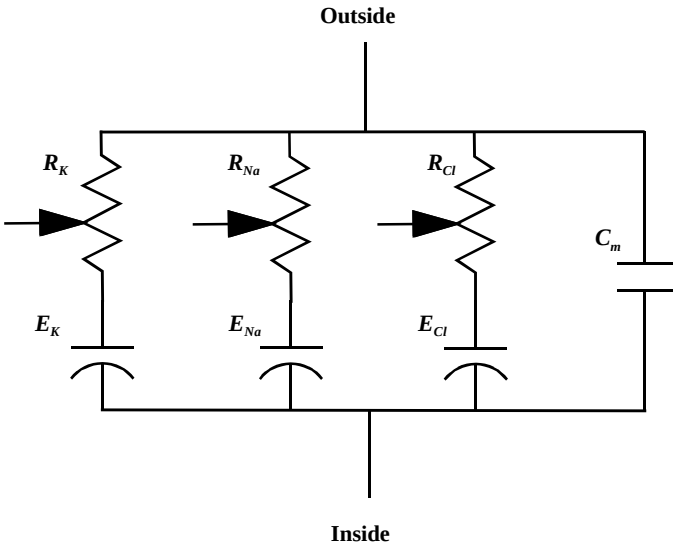

Fig 2.9.1 A simple model for a cell membrane. C_m=membrane capacitance, R_{Na}, R_K and R_{Cl} are resistances selective for respective ions and E_{Na}, E_K and E_{Cl} are equilibrium potentials for these ions.

In epithelial models the cell membrane model is usually further simplified by combining electromotive forces and resistances in direct current model (Fig 2.9.2) or with a resistance and with a capacitor in alternating current model (Kottra, Frömter 1990b).

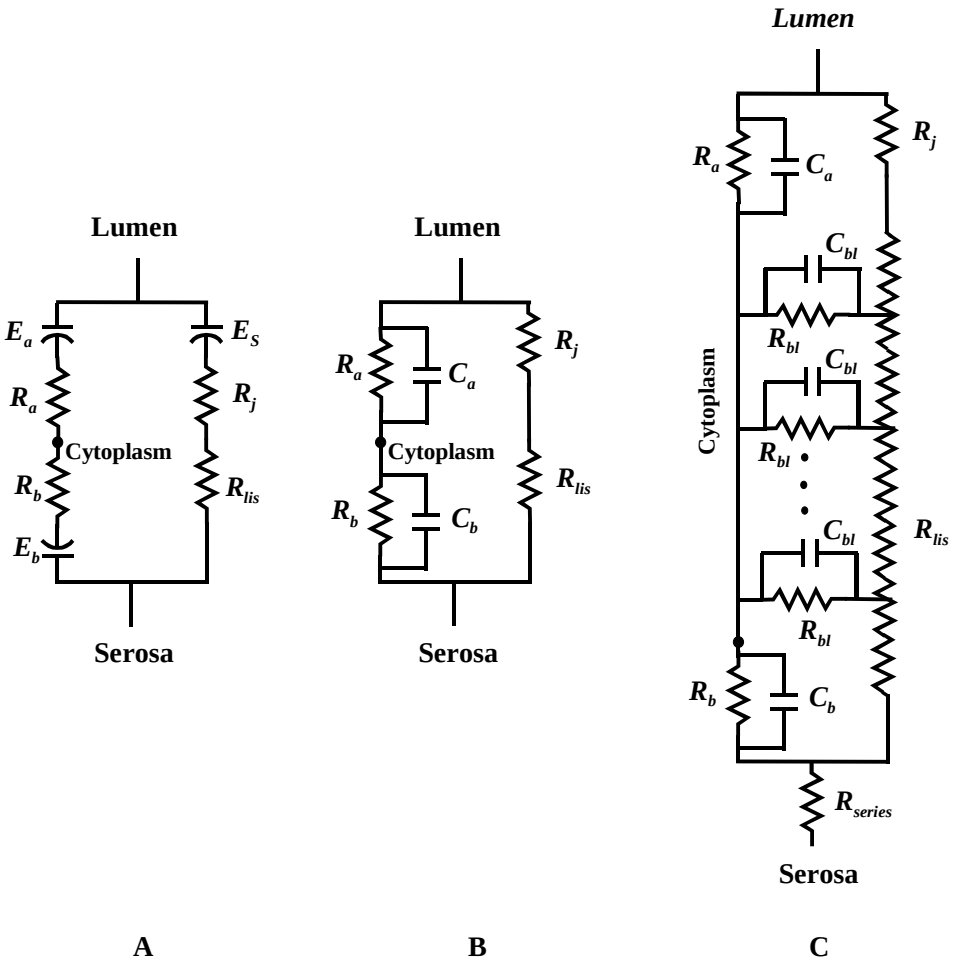

Fig 2.9.2 Simple electric models for an epithelium. R_j is tight junction resistance, R_{lis} is lateral intercellular space resistance, R_a is apical cell membrane resistance, R_b is basolateral cell membrane resistance, R_{bl} is basolateral cell membrane resistance to lateral intercellular space, R_{series} is submucosal resistance, E_a, E_b and E_s are respective electromotive forces, C_a and C_b cell membrane capacitances. A Direct current model, B Alternating current model C Lateral intercellular space is modelled with a distributed resistance.

The space between cells called lateral intercellular space (LIS) is usually very narrow, for example in mammalian urinary bladder it is 10 nm (Clausen et al. 1979). It can be modelled with a distributed resistance (Fig 2.9.2), if the lateral intracellular space is directly connected to basolateral solution and the inside of the cell can be assumed to be isopotential.

2.10 Measurement methods of passive electrical parameters of epithelia

2.10.1 Alternating one conductance component of the epithelium

In this method the model in figure 2.9.2A (lumped DC-model) is used. The transmucosal resistance (R_t) and the so called voltage divider ratio (a_{VDR}) are measured before and after application of an agent, which alter only one conductance pathway of the epithelium. Trans-mucosal resistance (R_t) and the voltage divider ratio (a_{VDR}) are measured by passing current pulses from a current pulse generator through the epithelium. The transepithelial potential deflection caused by the current pulse (ΔV_{sm}) is measured with a macro electrode connected to the serosal half-chamber using a similar mucosal half chamber electrode as a reference. The a_{VDR} is calculated as $\Delta V_{cm}/(\Delta V_{sm}- \Delta V_{cm})$, where ΔV_{cm} is a deflection of the apical cell membrane potential caused by the current pulse. One conductance pathway is altered either with inhibitors, transport activators or with ion substitutions. If only apical cell membrane resistance is altered the following equation can be deduced from the model (Reuss, Finn 1974)

$$R_s = \frac{R_t R_t^{'}(a_{VDR}^{'} - a_{VDR})}{R_t(a_{VDR}^{'} + 1) - R_t^{'}(a_{VDR} + 1)} \qquad [2.10.1]$$

$$R_b = \frac{R_t R_s}{(R_s - R_t)(a_{VDR} + 1)} \qquad [2.10.2]$$

$$R_a = a_{VDR} R_b \qquad [2.10.3]$$

, where the apostrophe denotes values obtained in the presence of alternating agent in the luminal solution.

In a second version of this method also the changes in membrane potentials are measured before and after conductance alternation (Frömter, Gebler 1977). For example if R_b is changed and E_a, E_s, R_a and R_s remain constant the following equations can be deduced:

$$R_s = \frac{R_t(a_{VDR}\beta + \beta - a_{VDR})}{(a_{VDR} + 1)\beta} \qquad [2.10.4]$$

$$R_a = \frac{a_{VDR} R_t R_s}{(a_{VDR} + 1)(R_s - R_t)} \qquad [2.10.5]$$

$$R_b = \frac{R_a}{a_{VDR}} \qquad [2.10.6]$$

, where $\beta=\Delta V_{cm}/\ \Delta V_{sm}$, ΔV_{cm} is the change of the apical cell membrane potential due to conductance change in the basolateral cell membrane and ΔV_{sm} is the change of transepithelial potential due to conductance change in the basolateral cell membrane.

The method assumes that the voltage divider ratio can be used as a measurement of apical to basolateral resistance ratio (R_a/R_b). In a leaky epithelium lateral intracellular resistance (R_{lis}) can seriously affect this assumption (see 5.7). The assumption, that only one conductance pathway is altered, is not necessarily valid and must be tested for each combination of an epithelium and an agent, individually. The changing of one conductance pathway changes also cell membrane potentials of all the cell membranes. Thus a change in the apical cell membrane conductance changes the basolateral cell membrane potential. If the basolateral cell membrane has voltage dependent ion channels also the basolateral cell membrane conductance is changed and the assumption for this model is not valid. The greater the change of a_{VDR} and the smaller R_s is compared to the cellular resistance (R_a+R_b) the more accurate the determination of R_s is (Kottra, Frömter 1990b). Temporally this method is relatively slow. Although the solution changes must be fast, it usually takes time to remove inhibitors completely from the epithelium. At best, the measurements can be repeated in order of a few minutes.

2.10.2 Impedance analysis

In these experiments transepithelial and intracellular voltage response to transepithelial series of sine wave currents are measured and impedance is calculated. With the aid of the Fourier transformation, the appropriate equations from the model in figure 2.9.2C are fitted to the obtained data (Kottra, Frömter 1984a). One of the most important and probably most difficult aspects of this method is that the equivalent circuit model must fit accurately to the measured impedance loci. Yet it should be as simple as possible. The measurement of leaky epithelia is difficult, because only a small fraction of the measurement current flow through the cell membrane producing small response (Kottra, Frömter 1990b). Therefore this method was further combined with the two-dimensional cable analysis. This produced more reliable estimates of R_a and R_b. This method is technically very demanding, because it combines the 2D cable analysis and impedance analysis and because shielded electrodes must be used. The temporal resolution

is in order of seconds and it allows the changes in membrane capacitances and the R_{lis} to be measured.

2.10.3 Two-dimensional intraepithelial cable analysis

The intraepithelial 2D-cable analysis can be used to measure resistive parameters from simple flat epithelia with low resistive junctional membranes. The continuous 2D-cable model treats the epithelium as a pair of thin parallel and uniform resistive sheets of infinite size separating a continuous intracellular space of uniform thickness. The flow of applied current is assumed to be equal in all directions within the epithelium's plane. A known current conducted to a point inside the epithelium causes a potential distribution, which obeys the following second order differential equation:

$$V(r)''+\frac{1}{r}V(r)'-\frac{V(r)}{\lambda^2}=0 \qquad [2.10.7]$$

where *V(r)* is potential at the distance of r from the intracellular current conducting electrode, lambda is the effective space constant and r is the distance from the intracellular current electrode.

The solution for this differential 2D-cable equation [2.10.7] is $V(r)=A\ K_0(r/\lambda)+ B\ J_0(r/\lambda)$, where K_0 and J_0 are modified Bessel functions of the second kind and zero order. $V(r)=0$ when $r\rightarrow\infty$, therefore B must be zero and the steady state ($t\rightarrow\infty$) solution for the differential 2D-cable equation is (Shiba 1971; Frömter 1972):

$$V(r) = A \cdot K_0\left(\frac{r}{\lambda}\right) \qquad [2.10.8]$$

where $A= \rho i_0/2\pi h$, $\lambda = \sqrt{R_m h / \rho}$ (λ is the space constant of the epithelium), K_0 is the modified Bessel function of the second kind and zero order, R_m = the cell resistance to the bath solutions, ρ = internal specific resistivity, h = thickness of the epithelium, r = distance from the current source and i_0 = applied current from the current passing electrode.

This solution to the 2D-cable equations is fitted to the measurements in order to obtain A and λ, and apical cell membrane (R_a), basolateral cell membrane (R_b) and shunt resistance (R_s) are calculated from the following equations:

$$R_m = 2\pi A \lambda^2 / i_0 \quad [2.10.9]$$

$$R_a = R_m(1+a_{VDR}) \quad [2.10.10]$$

$$R_b = R_m(1+a_{VDR})/a_{VDR} \quad [2.10.11]$$

$$R_s = R_t(R_a+R_b)/(R_a+R_b-R_t) \quad [2.10.12]$$

Where $a_{VDR} = R_a/R_b$ and R_t is transepithelial resistance.

This method requires fewer assumptions than the 2.10.1 methods and usually the measurement can be made in the linear range of cell membrane resistances. It should be remembered, that usually the current voltage relation of cell membranes is non-linear even in the physiological membrane voltage range (-100 to +50 mV). The main obstacle of this method is that it does not take lateral intracellular resistance into account. This might lead to severe underestimation of R_a/R_b (Boulpaep, Sackin 1980). If the resistance of gap-junction is high, this method cannot be used. Instead one should use a discrete model, such as that described in (Siegenbeek van Heukelom et al. 1972). An example of this method is given in Fig 4.2.1.

3. AIMS OF THE STUDY

The purpose of the present study was to develop measurement methods to elucidate the role of different defence mechanisms of the gastric mucosa against acid and ulcerogenic agents. The specific aims were as follows:

1) To develop a reliable and temporally fast method to measure different membrane resistances i.e. apical, basolateral cell membrane resistances and the shunt pathway resistance of the gastric antrum.

2) To study the effects of gastric acid on the cell membrane resistances and to explore the defence mechanisms of the gastric mucosa against luminal acid.

3) To study the effects of ulcerogenic compounds, such as ethanol, aspirin and taurocholic acid, on the gastric cell membrane resistances and to elucidate the early phases of the damage to the gastric mucosa.

4. MATERIALS AND METHODS

Necturi (Necturus maculosus) were obtained from St. Croix Biological Supplies, St. Croix, Stillwater, MN. In study I the Necturi were kept in filtered water at 4-6 ^{o}C. In studies II-IV the Necturi were kept in filtered water containing Methylene blue (Merck, Darmstadt, Germany) (1.0 mg/L) at 15-18 ^{o}C, and fed with compressed Chironomids once a day and before the experiments the animals were fasted for 1-2 days. They were anaesthetized by immersion in 1% tricaine methanesulfonate, and the antral portion of the stomach was resected, stripped of its seromuscular coat, and mounted, mucosal side up, in a perfusion chamber. The mucosal (volume 0.15 ml) and serosal (volume 0.15 ml) half-chambers were perfused at 25^{o} C from a reservoir individually at a rate of 1.5 ml/min, with pressure on the serosal side slightly negative to hold the tissue steady against its wire-mesh support. The exposed mucosal surface area was in both chambers 0.2 cm^2. After mounting, the tissues were allowed to stabilize for 30-60 minutes before start of the experiment.

All the animals received human care in compliance with the 'Principles of Laboratory Animal Care and the Guide for the Care and Use of Laboratory Animals´ formulated and prepared by the Institute of Laboratory Animal Resources and published by the National Institutes of Health (NIH publication no. 86-23, revised 1985). The authorization to perform this study was given by the Provincial Government of Uusimaa in accordance to Finnish legislation.

4.1 Solutions and chemicals.

The standard Ringer's solution contained (in mM): NaCl 87; $NaHCO_3$ 18; KCl 4; $CaCl_2$ 2; $MgCl_2$ 1; $KH_2PO_4^-$ 1 and glucose 10. This solution was gassed with 95% O_2 - 5% CO_2 having a steady-state pH 7.25 at 25^{o} C.

In study I the mucosal side of the epithelium was perfused with a similar Ringer's solutions as the basolateral side, but it was buffered to pH 6 with 10 mM MES (having 1 mM HCO_3^-). After satisfactory impalements of the cells, mucosal perfusion was continued with the Ringer's solution (without HCO_3^-) acidified to pH 3 with HC1. After a 15-20-min stabilization period, one of the

barrier-breaking agents, 10 mM taurocholate (TC), 20% (vol/vol) ethanol, or 10 mM acetylsalicylic acid, was added to the mucosal perfusate at pH 3 (study I).

In studies II –IV, at the beginning of each experiment the standard Ringer's solution was used for perfusion of both sides of the mucosa. The microelectrodes were positioned under microscopic control. In study III after 5 min of stable recordings, mucosal perfusion was continued with Ringer's solutions at pH 4.0, pH 3.5, pH 3.0 and pH 2.0 (methanesulfonate was substituted for HCO_3^-, adjusted with HCl or, in some experiments, with methanosulfonic acid). The perfusates were gassed with 95% O_2/5% CO_2. The serosal side was perfused with standard Ringer's solution (pH 7.25), unless otherwise stated. In the ion-substitution experiments Na^+ and Cl^- or NMDG (N-Methyl-D-Glucamine, Sigma) and Cl^- were substituted for all the ions in the standard Ringer's solution. These pure NaCl and NMDG-Cl solutions were used at three different pH values (pH 4.0, pH 3.5 and pH 3.0, adjusted with HCl or methanosulfonic acid). In sodium-free solutions NMDG was substituted for sodium. In the NH_4^+ preload experiments 20 mM sodium was substituted by NH_4^+ during the preload. Lowering the basolateral pH in one series of experiments was done by substituting methanosulfonate for HCO_3^-. The total HCO_3^- was changed from 18 mM to 6.5 mM and 11 mM, yielding a pH of 6.8 and of pH 7.0. Amiloride (0.1 mM, Sigma) was added to the solutions as indicated in the text. The pH 6.0 solution contained (in mM: NaCl 87; KCl 4; KH_2PO_4 1; $MgCl_2$ 1; 2-[N-Morpholino] ethane-sulfonic acid (MES) 10; Sodium-methanesulfonate 13.6; $CaCl_2$ 2 and glucose 10; it was titrated to pH 6.0 with NaOH.

In the study IV, five microelectrodes were positioned under microscopic control and, after stabilization of the recordings, mucosal perfusion was continued with low pH Ringer's solutions at pH 4.0 or pH 3.0. Thereafter mucosal perfusion was changed to low pH Ringer's solution containing 5%, 10% and 15% (vol/vol) ethanol (ETOH), respectively. The ion concentrations in all ethanol solutions were the same as in the corresponding solution, thus the control solution for ethanol was pure water as recommended (Singer 1983). In the pure NMDG-Cl solution $NMDG^+$ and Cl^- were substituted for all the ions in the standard Ringer's solution and the pH was adjusted to pH 3.0 with HCl. In 30 mM K^+ solution K^+ was substituted for Na^+. In 52.4 mM Na^+ solution $NMDG^+$ was substituted for Na^+ and in the 54 mM K^+ solution K^+ was further substituted for $NMDG^+$. These low Na^+ and high K^+ solution were used sequentially. In 9 mM Cl solutions gluconate was substituted for Cl^- and 5 mM calcium gluconate was added to compensate the

calcium binding to gluconate. The change of agar-KCl electrodes liquid junction potential due to solution change to low Cl^- solution was corrected according to Henderson formalism (Amman 1986). The perfusates were gassed with 95% O_2/5% CO_2. The serosal side was perfused with standard Ringer's solution (pH 7.25), unless otherwise stated. Amiloride, quinine, tetraethylammonium (TEA), anthracene-9-carboxylix acid (AC-9) and 5-Nitro-2- (3-phenylpropylamino) benzoic acid (NPPB) (Sigma-Aldrich, St Louis, MO), were used as indicated in the text.

4.2 Two dimensional-cable analysis

The intraepithelial 2D-cable analysis can be used to measure resistive parameters from simple flat epithelia with low resistive junctional membranes (Fig 4.2.1). The steady state ($t \rightarrow \infty$) solution for the differential 2D-cable equations is given in [2.10.8].

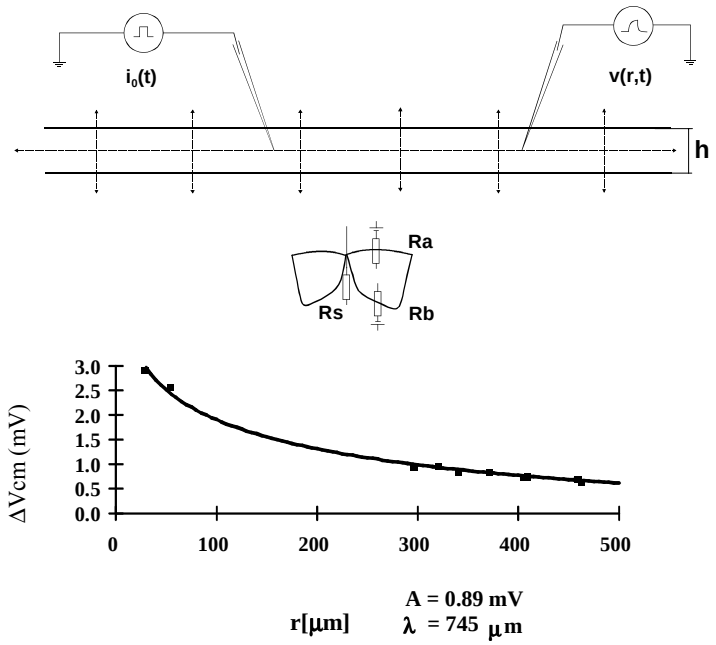

Fig 4.2.1 A schematic drawing of a 2-dimensional cable. Cross section (top), a lumped model with only the transepithelial resistance components shown (middle), and an example measurement with 5 electrodes giving 10 measurement points (dots), continuous line is the solution to the 2D-cable equations fitted to the measurements (bottom). Current flows are indicated by arrows. Under the assumptions given in the text, the epithelium can be modelled as a Hevisides's Bessel cable.

The solution to the 2D-cable equations [2.10.8] was fitted to the measurements in order to obtain A and λ, and apical cell membrane (R_a), basolateral cell membrane (R_b) and shunt resistance (R_s) were calculated from the equations [2.10.9]-[2.10.12].

4.2.1 Confidence limits for parameter values obtained by fitting

Asymptotic standard errors (SE) can be calculated for the fitted parameters by the following equation (Bates, Watts 1988; Seber, Wild 1988):

$$\beta_p \pm s\sqrt{[(X^T X)^{-1}]_{pp}} \qquad [4.2.1]$$

where β_p are the fitted parameters (β_0=A, β_1 = λ), X is a derivative matrix defined below (superscripts T and -1 indicate transpose and inverse matrix, respectively) s is square root of the residual mean square. Asymptotic (1-α) confidence limits can be obtained by multiplying the SE by the upper $\alpha/2$ quantile for Student's T distribution with N-2 degrees of freedom. N is the number of voltage response measurements along the distance scale. The derivative matrix is:

$$X = \begin{bmatrix} K_0\left(\frac{r_1}{\lambda}\right) & \frac{r_1 \cdot A \cdot K_1\left(\frac{r_1}{\lambda}\right)}{\lambda^2} \\ \vdots & \vdots \\ K_0\left(\frac{r_N}{\lambda}\right) & \frac{r_N \cdot A \cdot K_1\left(\frac{r_N}{\lambda}\right)}{\lambda^2} \end{bmatrix} \qquad [4.2.2]$$

where K_1 is a modified Bessel function of the second kind and first order and r_N is distance. The asymptotic confidence regions were found to be nearly identical to exact confidence regions and thus the asymptotic confidence regions can be used in optimisation.

The confidence limits of the calculated parameters can be deduced with simple rules of the error analysis (Bevington 1969; Taylor 1982). The confounding error term for R_m is:

$$R_m^{err} = \sqrt{\left(\frac{2\pi\lambda^2}{i_0} A_{err}\right)^2 + \left(\frac{4\pi A\lambda}{i_0} \lambda_{err}\right)^2} \qquad [4.2.3]$$

where sub- or superscript 'err' means the confidence limit for the parameter.

4.2.2 Experimental setup for two dimensional cable analysis

Four/five nearby surface epithelial cells were impaled with four /five conventional microelectrodes under microscopic control and using two hydraulic (water) micromanipulators (Narishige, Tokyo, Japan) and two/three mechanical micromanipulators (Prior, Hertfordshire, England), The electrodes were manufactured by pulling borosilicate tubing with fiber (GC150F-15, Clark Electromedical Instruments, Pangbourne, GB) with a microelectrode puller (P-87, Sutter, Novato, CA, USA) into micropipettes (outer tip diameter < 0.5 μm) which were then filled with a solution containing 0.6 M KCl and 0.8 M Na-acetate. An Ag-AgCl reference electrode was connected to the mucosal half-chamber via an agar-KCl bridge. Impalement of the apical cell membrane was manifested as an immediate negative change in the microelectrode reading and as a change in the magnitude of the voltage deflections induced by current pulses passed across the mucosa.

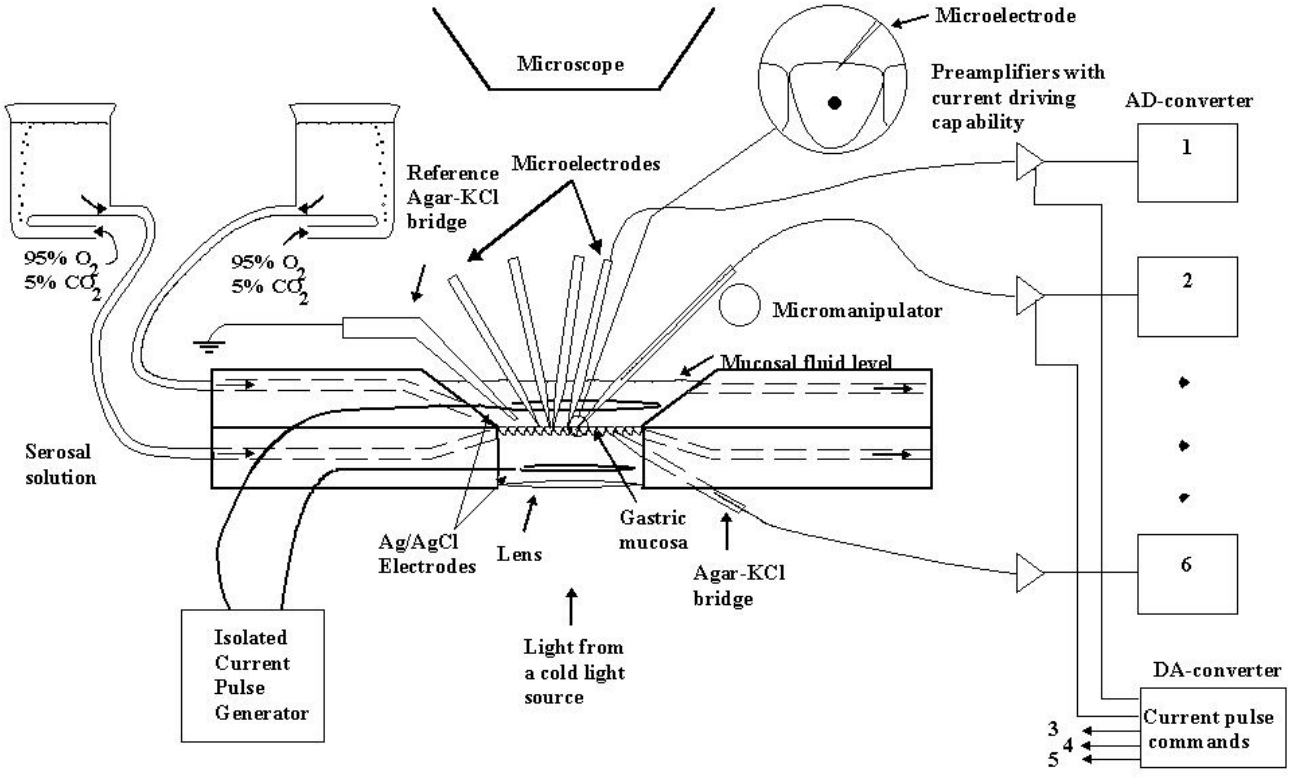

Fig. 4.2.2 A schematic drawing of the experimental setup. The epithelium is perfused continuously on both sides and impaled with five microelectrodes under microscopic control. All the electrical connections are not shown. Not drawn into the scale.

Transmucosal resistance (R_t) and the ratio of apical and basolateral membrane resistances (R_a/R_b) were measured by passing current pulses of (40-50 μA/cm^2) from a current pulse generator through the epithelium by means of two circular Ag-AgCl electrodes located in the mucosal and serosal half-chambers. The transepithelial potential deflection caused by the current pulse (ΔV_{sm}) was measured with an Ag-AgCl-electrode connected to the serosal half-chamber via an agar-KCl bridge using a similar mucosal half chamber electrode/agar-KCl-bridge as a reference. The R_a/R_b was calculated as

$$\Delta V_{cm}/(\Delta V_{sm} - \Delta V_{cm}) \qquad [4.2.4]$$

, where ΔV_{cm} is a deflection of the apical cell membrane potential caused by a current pulse. It was calculated for each one of the four/five electrodes by a computer and the mean was used as the ratio of apical and basolateral membrane resistances in the final calculations. The R_a/R_b for single electrodes was also used to get further evidence for proper impalements. The measurements of R_t and R_a/R_b were corrected for chamber resistance. The distances between the electrodes were measured using an ocular micrometer with one μm graduation at total magnification of 105.

For the intraepithelial 2D-cable analysis, current pulses (6.5-20 nA) were passed through one electrode while measuring the voltage responses with the others. In order to obtain six independent voltage deflection measurements along the distance scale with four electrodes, the intraepithelial current was passed through a different electrode during every measurement step. In the first measurement step, voltage deflections for three different distances were measured. In the second measurement step, the voltage deflections for two new distances and, in the third step, for one new distance were obtained. If the fifth electrode was used, the measurement was repeated four times and in every step one more distance would be measured as compared with the four electrode setup, giving a total of ten independent distances. At the same time confirmation of the measurements was obtained because three (five) of the six (ten) different voltage deflections were measured in both directions, and they should yield equal results to fulfil criteria for continuation of the experiment.

Two different current strengths were used automatically to find out possible undesired unlinearity problems, e.g. rapid changes in membrane resistances, electrode blockages during the

measurement or possible deviations from linearity in membrane resistances. The measurements were averaged on two different levels. First, measuring voltage deflections in response to intracellular current pulses, the voltages before and during the pulse were averaged (usually 100 ms, 4ksample/s/channel or synchronized to 50 Hz) and these averaged voltage measurements were subtracted to get voltage deflection. Secondly, the intracellular current pulses could be repeated n times and the voltage deflections could be averaged to increase the signal/noise ratio by $\sqrt{n}$. The possible blockade of the electrodes was monitored in the current passing electrode during the current pulse by observing the electrode voltage continuously. If the electrode would be blocked, the current source would saturate and enough current would not be delivered.

The time used for a measurement depends on the epithelium, electrodes (noise and number of electrodes used) and distance configuration. The epithelium acts as an R-C unit and has its intrinsic time constant. The longer distance the response is measured the slower is the rise time of the signal. The higher the electrode resistance the noisier is the response and more averaging is required. From the measurements it was deduced that a measurement 600 ms after the initiation of an intraepithelial current pulse (i_o=13 nA) could be usually safely used to measure the dc resistance of the *Necturus* antrum. Time resolution under 9 s of the whole 2D-cable measurement can be achieved under the following assumptions: 1) only time window averaging is used, 2) 600 ms is enough for the voltage response to rise, 3) only one current strength and five electrodes are used. If subsequent voltage deflections are averaged, approximately 5.5 s will be added to the measurement time for every averaging step.

The computer program controlled the measurement equipment and automatically performed a 2D cable measurement. A measurement included passing of transepithelial current pulse, digitizing, calculating and storing of the results (V_{cm}, V_{sm}, ΔV_{cm}, ΔV_{sm}, R_t, R_a/R_b), passing intraepithelial current through microelectrodes one at a time and digitizing and storing the voltage responses. An example of the measurement is shown in Fig 4.2.1 and a schematic drawing is presented in Fig 4.2.2.

4.3 Amiloride exposure technique

To get an estimate of intraepithelial resistances the amiloride exposure technique (Ashley et al. 1985) was used in a series of experiments. The basic assumption in this method is that amiloride added to the luminal solution selectively blocks the apical cell membrane ion channels, presumably Na^+-channels. This assumption is supported by a sudden hyperpolarization of the apical cell membrane potential, by a sudden increase of the R_a/R_b and by the reversibility of these effects when amiloride is removed from the luminal solution. On this premise the intraepithelial resistances can be calculated from equations [2.10.1]-[2.10.3]. The R_a/R_b and R_t were measured as described in 4.2.2 before and after exposure to luminal 0.1 mM amiloride. In study I the measurements were performed before and after 5 minutes exposure to the test agent (taurocholate, ASA or ethanol). The test agent was first washed out and the mucosa was then exposed to standard Ringer's solution and thereafter to Ringers's solution with 0.1 mM amiloride. In study II both sides of the epithelium were perfused with stadard Ringer's solution and amiloride 0.1mM was added to the luminal solution.

4.4 Measurement of intracellular pH

Intracellular pH was measured with a double-barrelled microelectrode having a liquid sensor pH-sensitive barrel and a PD barrel. In short, borosilicate tubings with fiber in both barrels (2 GC 150F-15, Clark Electromedical, Pangbourne Reading, GB) were pulled into micropipettes with an outer tip diameter < 0.5 μm. The pH-selective barrel was silanized with N, N-Dimethyltrimethyl-silylamine (Fluka, Buchs, Switzerland) vapor at 140°C. The filling solution contained 150 mM NaCl and 200 mM N- [2-Hydroxyethyl]piperazine-N'-[2-ethanesulfonic acid](HEPES) at pH 7.5, and the liquid proton sensor was the "Hydrogen Ion Ionophore II Cocktail A" of Fluka (Buchs, Switzerland). The other barrel, filled with 0.6 M KCl and 0.8 M Na-acetate, was used for measurement of the apical transmembrane potential (V_{mc}). The electrodes were calibrated in a series of Ringer solutions containing 10mM HEPES or MES before and after each experiment. Proton selectivity of these electrodes is good with negligible interference from other ions, and the response of the microelectrodes is linear over a pH-range of 2.0-9.0 (Chao et al. 1988). Our microelectrodes had an average slope of 52.0 ± 1.4 mV/pH-unit (N=12). The tip resistance of the pH-barrel was 100-200 GΩ and of the PD-barrel 20-40 MΩ. The electrometer amplifier used with the pH-selective barrel had an input bias current $<10^{-13}$A and input impedance $>10^{15}$ Ω. The signals of the pH-

selective barrel (H^+ activity + apical transmembrane PD) and the PD barrel (apical transmembrane PD) were subtracted to give the net H^+ activity signal.

4.5 Measurement of intracellular sodium.

Intracellular Na^+ activity (a_{Na}^i) was measured with separate single-barrelled microelectrodes. The Na^+ selective electrodes were manufactured and handled as were the pH-microelectrodes, except that the liquid sodium sensor was the "Sodium Ion Ionophore I - Cocktail A" of Fluka (Buchs, Switzerland), and the tubing was single-barrelled (GC150F-15, Clark Electromedical, Pangbourne Reading, GB). The PD electrode was manufactured as described above. Two nearby cells were impaled with the electrodes. In order to assure that both electrodes were in the surface cells, a long current pulse was conducted through the epithelium, and the voltage step response from the current pulse was recorded from both electrodes. This recording was not done until steady state values were obtained in both electrodes. The measurement was performed repeatedly and automatically. In order to accept the a_{Na}^i measurement, only a few mV (1-2mv when the total magnitude was approximately 30mV) difference was allowed.

Na^+-selective electrodes were calibrated in a series of NaCl solutions with different Na^+ activity (0.1, 1, 5, 10, 50 mM) at constant ionic strength (150mM) with K^+ as the Na^+ substitute. An activity coefficient of 0.75 was used to convert Na^+ concentrations into activities. The mean response of the microelectrodes was 20.6 ± 1.9 mV upon a Na-activity change from 1 to 5 mM, 12.4 ± 0.5 mV from 5 to 10, and 35.9 ± 0.9 mV from 10 to 50 mM (N=9). The derived tenfold slopes were 29.4 ± 2.7 mV, 41.3 ± 1.8 mV and 51.3 ± 1.3 mV, respectively. The Na^+-electrodes had an average resistance of 155 ± 29 GΩ and the PD electrodes 21 ± 2 MΩ. The a_{Na}^i values were derived from the calibration curves, using the appropriate range of the calibration. Interference by K^+ was estimated by determining the selectivity coefficient for Na^+ over K^+ ($K_{Na,K}$) using the fixed interference method (fixed 150 mM KCl background concentration). The mean selectivity coefficient was log $K_{Na,K}$ = -1.71 ± 0.03 (N = 10). When the above calibration method is used, interference by K^+ is small. Interference by Ca^{2+} is known to be high (log $K_{Na,Ca}$ = 0.2) (Amman 1986) and if intracellular Ca^{2+} activity rises well above μM level, it should be corrected. No correction was made for possible Ca^{2+} interference. The signals of the Na^+-selective electrode (Na^+ activity + apical transmembrane PD) and the PD electrode (apical transmembrane PD) were subtracted to give the net Na^+ activity signal.

4.6 Measurement of changes in cell volume

The cell volume changes were monitored measuring intracellular tetramethylammonium (TMA) activity with TMA-selective microelectrodes (Reuss 1985). TMA is a large molecule, which does not readily leak out of the cell, thus allowing fast changes in cell volume to be recorded. Before the experiment TMA was loaded into the cells with a long (1.5-2 hours) exposure to 50mM TMA (substituting for Na^+) in Ringer's solution. A similar loading technique has been used in frog retinal pigment epithelium (Adorante 1995). During the experiment a low concentration of TMA (2mM) was added in all solutions in order to decrease the TMA gradient between the cell interior and perfusion solutions, thus minimizing the leakage.

TMA selective electrodes were manufactured as follows. Borosilicate tubings with fiber (GC 150F-15, Clark Electromedical, Pangbourne Reading, GB) were pulled into micropipettes with an outer tip diameter < 0.5 μm. and silanized with N, N-Dimethyltrimethyl-silylamine (Fluka, Buchs, Switzerland) vapor at 140°C for 3 hours. The filling solution contained 50 mM TMA-Cl and 200 mM N-[2-Hydroxyethyl]piperazine-N'-[2-ethanesulfonic acid] (HEPES) at pH 7.5. The liquid K^+ sensor used was potassium tetrakis (p-chlorophenylborate) based ionophore IE190 (WPI, Sarasota, FL, equivalent to Corning 477317). These electrodes are far more sensitive to TMA^+ than K^+ (selectivity coefficient (TMA^+/K^+) is $0.9 \cdot 10^3$) (Reuss 1985). TMA selective electrodes were calibrated in a series (1 to 50mM) TMA solutions at fixed 105mM KCl background. The mean slope from 5 to 50mM TMA activity was 56.1±5.2mV. The signals of the TMA-selective electrode (TMA^+ activity + apical transmembrane potential) and the conventional electrode (apical transmembrane potential) were subtracted to give the net TMA^+ activity signal (E_{TMA}). The relative cell volume change was calculated from

$$10^{(E^0_{TMA} - E^t_{TMA})/Slope} - 1 \qquad [4.6.1]$$

where *Slope* is the slope of the electrode, E^0_{TMA} is the TMA^+ activity signal at the reference point and E^t_{TMA} is the signal after volume change. Thus 1mV change in the TMA^+ activity signal corresponds approximately to a 4% volume change. In preliminary experiments ±25% change in osmolarity caused a maximal volume change between –27±6% and 10±4%.

4.7 Statistics

The results are given as mean ± SEM. Statistical analysis of the raw data was performed with Student's t-test for paired and unpaired variates. Probability values of less than 0.05 were considered significant. The difference between the measurement methods in each parameter was tested against lower and upper tolerance limits with one-sided Student’s t-test. The differences between basal and amiloride values were tested with 2-tailed Student’s t-test for paired variates. P values of <0.05 were considered significant.

5. RESULTS

5.1 Effect of luminal 10 mM taurocholate on membrane parameters (I)

Addition of 10 mM taurocholate to the mucosal perfusate (pH 3.0) caused an almost immediate acidification of pH_i, pH_i decreasing from 7.21 ± 0.02 to 6.05 ± 0.27 ($p < 0.01$, $n = 9$) in 30 min. Exposure to luminal 10 mM taurocholate at pH 3.0 induced a significant and almost parallel decrease of V_{cm} and V_{cs}. V_{cm} decreased from -40.2 ± 3.58 to -4.1 ± 0.7 mV ($p < 0.01$, $n = 5$) and V_{cs} from -44.5 ± 4.1 to -8.1 ± 1.7 mV ($p < 0.01$, $n = 5$) in 30 min. In contrast, V_{ms} stayed relatively stable, V_{ms} changing from -4.3 ± 0.9 to -4.0 ± 0.5 mV during the experiment.

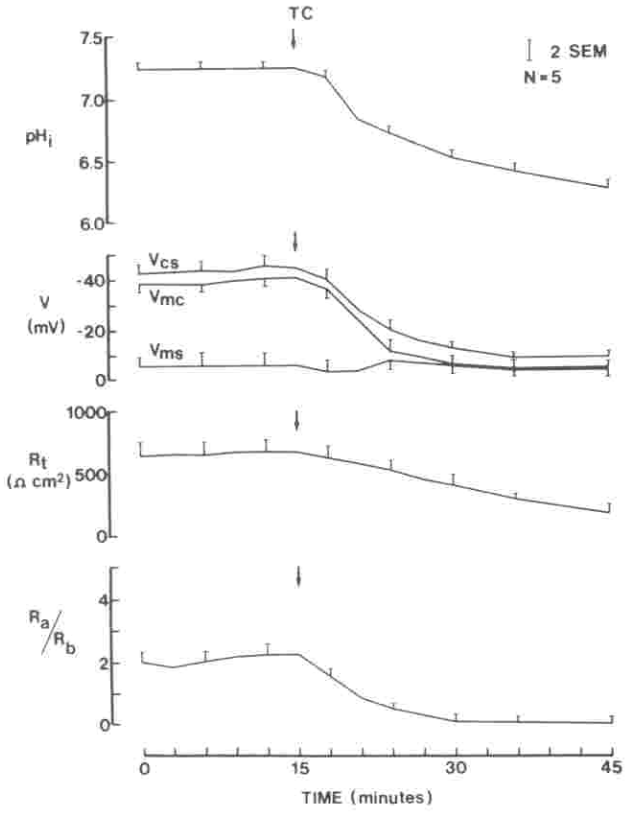

Fig 5.1.1 Effect of 10 mM taurocholate at luminal pH 3.0 on intracellular pH and epithelial electric potentials and resistances. In pH_i, data only from the experiments where the electric parameters also were measured.

In R_t a progressive decline was seen after exposure to 10 mM taurocholate, R_t decreasing from 647 ± 81 to 174 ± 50 Ohm cm^2 in 30 min ($p < 0.01$, $n = 5$). An immediate decrease also occurred in R_a/R_b after exposure to 10 mM taurocholate, R_a/R_b decreasing from 2.17 ± 0.42 to 0.38 ± 0.02

within the first 15 min, where after the ratio further decreased close to zero till the end of the experiment (Fig 5.1.1). In a separate series of experiments the influence of 10 mM taurocholate on the absolute values of intraepithelial resistances was determined. A 5-min exposure to 10 mM taurocholate promoted a profound and significant ($p < 0.05$) decrease in R_m (from 7712 ± 922 to 2912 ± 250 Ohm cm^2, $p<0.05$,N=5), the effect being somewhat stronger on R_a (from 5866 ± 812 to 2103 ± 293 Ohm cm^2, $p<0.05$, N=5) than on R_b (from 1846 ± 114 to 809 ± 181 Ohm cm^2, $p<0.05$, N=5). R_s remained unaffected.

5.2 Effect of luminal 10 mM ASA on membrane parameters (I)

Exposure of the mucosa to 10 mM ASA at pH 3.0 induced a biphasicresponse in pH_i. During the first 6-9 min, pH_i alkalinised from 7.20 ± 0.03 to 7.39 ± 0.60 ($p < 0.01$, n = 11).

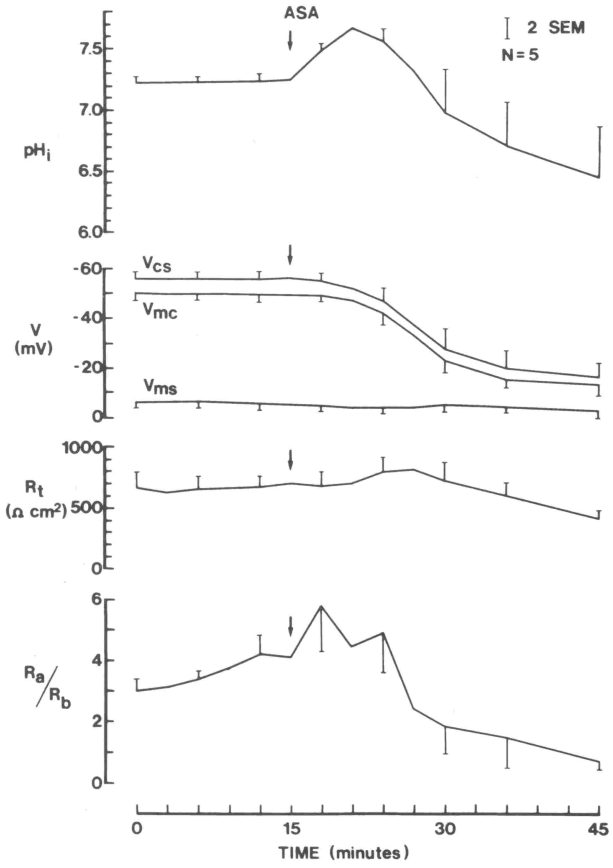

Fig 5.2.1 Effect of 10 mM ASA at luminal pH 3.0 on intracellular pH and epithelial electric potentials and resistances. In pH_i, data only from the experiments where the electric parameters also were measured.

This initial alkalinisation was followed by a progressive acidification of pH_i from 7.39 ± 0.60 to 6.32 ± 0.14 during the next 10-15 min ($p < 0.01$), and then further by a slower acidification to 6.10 ± 0.09 until the end of the experiment. V_{cm} and V_{cs} remained initially relatively stable, but after a delay of 4-6 min a profound decline of V_{cm} and V_{cs} occurred. V_{cm} decreased from -50.6 ± 2.1 to -14.5 ± 5.8 mV and V_{cs} from -55.8 ± 2.4 to -20.4 ± 7.0 mV ($p < 0.01$, n = 5) in 30 min. In contrast, V_{ms} remained stable during the whole experiment (V_{ms} from -5.2 ± 0.41 to -5.9 ± 1.37 mV). R_t slightly increased during the first 15 min after exposure to 10 mM ASA (R_t from 694 ± 116 to 728 ± 138 Ohm cm^2, whereafter it decreased to 410 ± 62 Ohm cm^2 ($p < 0.05$) during the next 15 min. R_a/R_b also showed an initial increase during the first 6-9 min (from 4.15 ± 0.67 to 5.87 ± 1.27, $p < 0.01$}, whereafter a progressive decline to 0.76 ± 0.18 ($p < 0.01$) occurred (Fig 5.2.1). A 5-min exposure moderately, but not significantly, increased R_m (from 3835 ± 556 to 4943 ± 674 Ohm cm^2, NS, N=5) and R_a (from 2323 ± 572 to 3037 ± 587 Ohm cm^2, NS, N=5) and increased significantly R_b (from 1512 ± 166 to 1906 ± 160 Ohm cm^2, $p<0.05$, N=5). In R_s slight but insignificant decreases were noted (from 829 ± 193 to 757 ± 154 Ohm cm^2, NS, N=5).

5.3 Effect of luminal 20% ethanol on membrane parameters (I)

In 11 experiments, pH_i remained relatively stable during the first 4-6 min after exposure to 20% (vol/vol) ethanoI at pH 3.0, whereafter a progressive acidification was recorded. pH_i decreased from 7.24 ± 0.01 to 6.34 ± 0.12 ($p < 0.01$, n = 11) within the first 15 min after exposure to 20% ethanol, whereafter a slower decline to 6.11 ± 0.11 occurred during the next 15 min. Exposure to luminal 20% ethanol initially caused a hyperpolarization of V_{cm} and V_{cs}, V_{cm} increasing from -41.2 ± 1.7 to -53.2 ± 3.7 mV, and V_{cs} from -45.7 ± 2.2 to -58.3 ± 3.1 mV ($p < 0.01$, n = 5) within the first 3-6 min. Thereafter, a progressive decline of both parameters occurred, and after 30 min V_{cm} was decreased to -14.5 ± 1.7 and V_{cs} to -17.5 ± 2.7 mV. In V_{ms}. a slight but statistically, insignificant decrease occurred during the experiment (V_{ms} from -4.5 ± 0.73 to -3.0 ± 1.3 mV). Exposure to luminaI 20% ethanol caused an immediate decrease in R_t, R_t decreasing from 727 ± 44 to 261 ± 35 Ohm cm^2 during the 30 min exposure ($p < 0.01$). In contrast, R_a/R_b remained relatively stable during the first 4-6 min. whereafter an abrupt reduction

of the ratio occurred, R_a/R_b decreasing from 4.00 ± 0.51 to 1.40 ± 0.34 ($p < 0.01$) within the next 3-4 min. This was followed by a slower decline to 0.34 ± 0.13 until the end of the experiment (Fig 5.3.1). A 5-min exposure to 20% ethanol induced a rather strong, but yet insignificant decrease in R_m (from 6493 ± 1134 to 3775 ± 784 Ohm cm^2, NS, N=5). The effect was mainly directed to R_a, where a significant decrease was observed (from 4660 ± 938 to 2202 ± 593 Ohm cm^2, $p<0.05$, N=5), whereas the effect on R_b was much smaller (from 1833 ± 479 to 1573 ± 232 Ohm cm^2, NS, N=5). A significant ($p < 0.05$) decrease was also observed in R_s (from 697 ± 95 to 505 ± 88 Ohm cm^2, $p<0.05$, N=5).

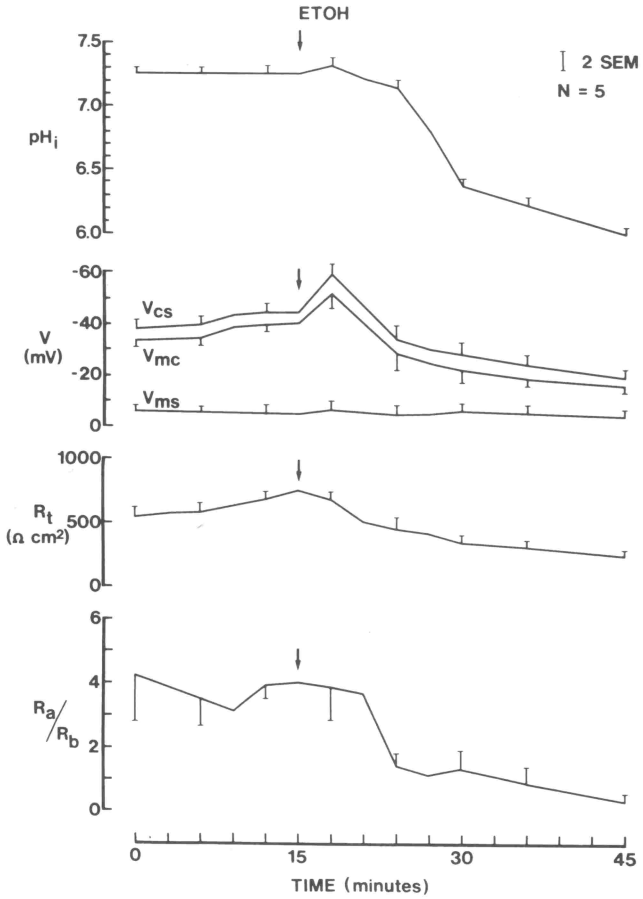

Fig 5.3.1 Effect of 20% (vol/vol) ETOH at luminal pH 3.0 on intracellular pH and epithelial electric potentials and resistances. In pH_i, data only from the experiments where the electric parameters also were measured.

5.4 Measuring the unlinearity of voltage response to intracellular current (II)

In these experiments the linear range of response to intracellular current in nearby cells was explored to find out a safe linear range of intracellular current for the *Necturus* antrum. Some

unlinearity was observed already at 30nA as seen in Fig 5.4.1. One assumption in the intraepithelial two dimensional cable analysis is that the current spreads equally in all directions along the plane of epithelium. This can be tested roughly in every measurement if the electrodes are placed similarly as in Fig 5.5.3 d. The epithelia, in which uniform current spread is not observed, will be discarded. In the present measurements the unequal spatial distribution of current spread was usually not a problem.

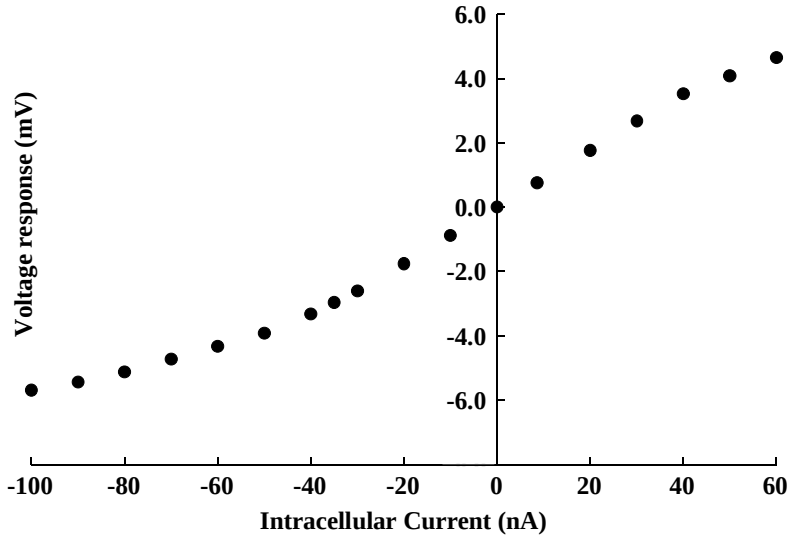

Fig 5.4.1 Unlinearity of voltage response to intracellular current. Voltage response to intracellularly applied current at a distance of 540 μm from the current passing electrode. Ordinate: Apical cell membrane potential deflections caused by intracellular current. Abscissa: Intracellular current passed by the current passing electrode.

5.5 Optimised Relative Positioning of Electrodes (II)

It is important to know how the relative positioning of electrodes should be chosen in order to minimize the error. Clearly the first measuring distance (r1) should be at most a few cell diameters. It is not preferred to impale them in the same cell, because it is difficult to obtain stable two-electrode recordings from a single cell. Also the error of the continuous model will grow and the discrete model should be used if two electrodes are impaled in the same cell or even adjacent cells.

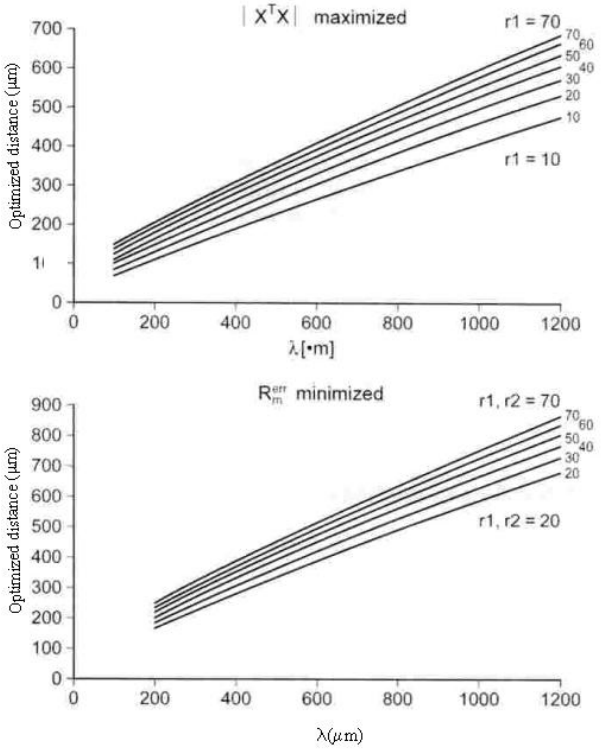

Fig. 5.5.1 Optimised distances for different λ. Two different optimisation methods were examined, namely maximizing $|X^TX|$ and minimizing the error of R_m. The value of A does not affect the optimised distances.

a.) Maximizing $|X^TX|$: The optimised second distance (r2) is shown for different r1. r1 is from 10 to 70 μm at 10 μm intervals. If the initial guess of λ is correct half the distances are near r1 and the other half near r2. r1 is the smallest distance used. The figure can be used as a starting point for a sequential optimisation with this method. Measure r1 and select r2 and r3 to be near the optimised r2.

b.) The theoretical end result of minimizing the error of R_m for 10 points measurement: If the initial guess of λ is correct, r2 is near r1 and the other eight distances are near the optimal distance shown in the figure. r1 and r2 are from 20 μm to 70 μm at 10 μm intervals. If the λ of the epithelium measured is known from a previous measurement, this figure might be helpful in selecting new distances, because a small scatter in the longer distance does not substantially increase the error (see Fig 5.5.2, curves 4 and 7).

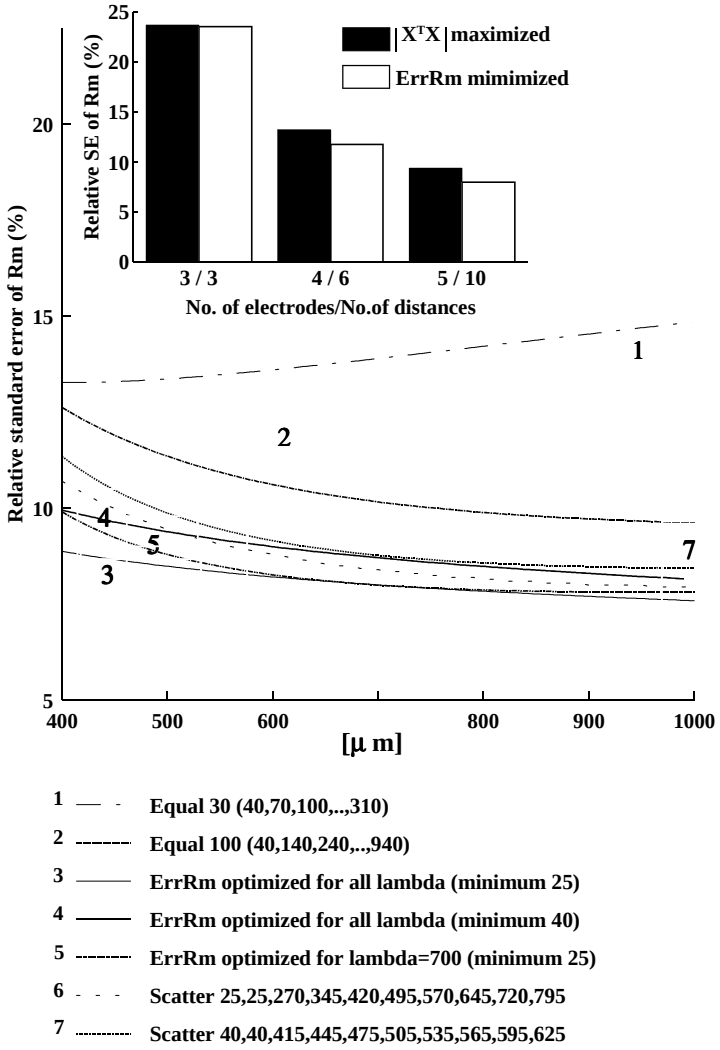

Fig 5.5.2 Relative standard error of R_m for different distance configurations. The error of R_m in those distance configurations, where the distance between each successive measurement point is equal (e.g. 30 µm, curves 1-2), is decreased when this equal distance is increased up to 95 µm. The solid curves of the picture show the error when the distances are optimised for every lambda by minimizing the error of R_m (ErrRm). The effect of decreasing the shortest distance from 40 µm to 25 µm is shown in curves 3 and 4. The scattered approach curves (6-7) are optimised by minimizing the error in R_m but forcing the scattering (λ=700). The minimum distance used for each curve is given in the figure and all curves are calculated for 10 points measurements. In the insert the effect of increasing measurement points and also different optimising methods are compared (A=1, λ=700, minimum distance=25 µm). For drawing purposes s=0.086, 0.061 and 0.056 for 3,6 and 10 points measurements, respectively.

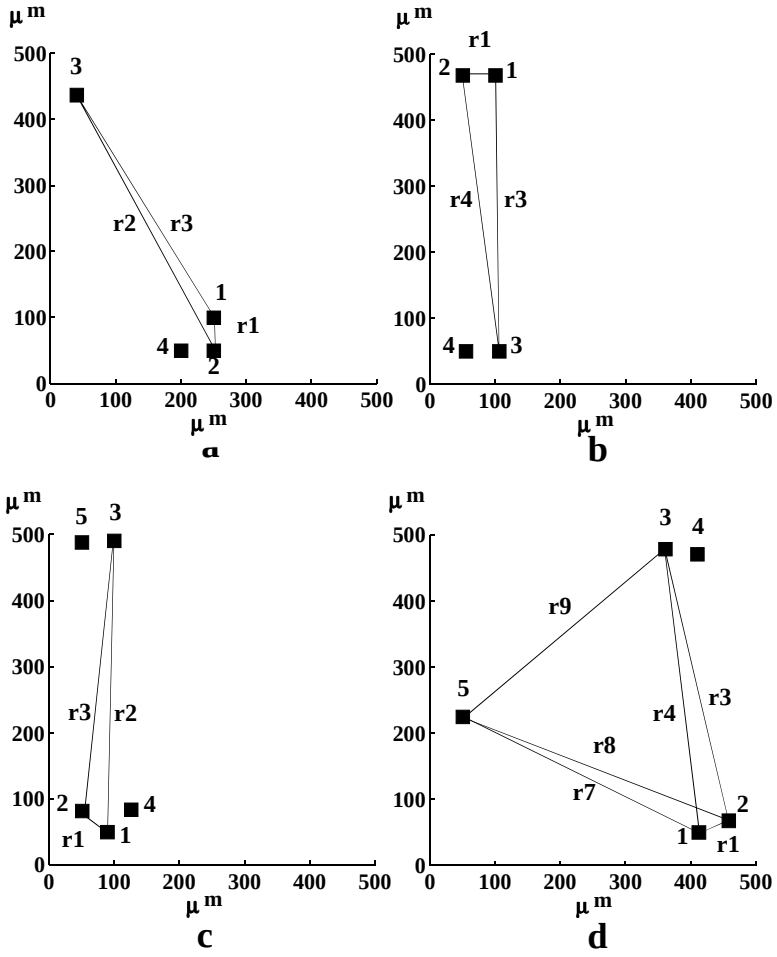

Fig 5.5.3 Four distance configurations referred to in the text. Top view, origo is arbitrary. Figures a and b are for four electrodes set-up, c and d for five electrode set-up. Squares are positions of electrode tips in the epithelium. For clarity only a few distances (continuous lines) are shown (r1,r2...). Plain numbers are labels assigned to each electrode.

In sequential optimising design one first estimates the parameters with a few distances and thereafter the new distances are optimised based on the obtained results. In the derivative matrix X the new distances are included as variables and the determinant of $X^{T}X$ (Seber, Wild 1988) is maximized or the equation [4.2.3] is minimized with respect to these new distances. In both methods, r1 should be as small as possible (for limitations, see above).

If the initial guess of λ is right, the result from maximizing $|X^{T}X|$ is straightforward, half the distances are close to r1 and the other half are near the optimal distance r2 shown in Fig 5.5.1 a. Minimizing the equation [4.2.3] gave theoretically slightly better results (insert in Fig 5.5.2.) and a different optimal distance configuration. If the initial guess of λ is correct, the second distance

(r2) is near r1 and the other eight are near the optimal distance shown in Fig 5.5.1 b. Similar curves can be calculated for the six points measurement. Due to electrode positioning the scatter of measurement points is inevitable, but even a quite strong scatter in the longer distance as in the curve 6 in Fig 5.5.2 is tolerable. In Fig 5.5.3 some relative positions of electrodes are shown.

5.6 Number Of Measuring Points (II)

If the number of measuring points is increased from six to ten, theoretically the SE of R_m is decreased by 29% (A=1, λ=700) as shown in the insert of Fig 5.5.2. Because all the measurements give two measured values for each distance, it would be tempting to use these measurement points as a replication, which would allow doubling the amount of measurement points. Those extra values are however rather reconfirmations than genuine repeated points. They will decrease that part of s, which is related to the precision of voltage measurements. Thus they can be included in the fitting process, but when calculating error terms, only the average of obtained voltage in both directions should be used.

5.7 Error of R_a/R_b (II)

When R_a/R_b is calculated from equation [4.2.4] it is underestimated if large potential differences are generated in the lateral intracellular space (LIS) induced by the measuring current. These potential differences may be formed if the resistance ratio of the tight junction and lateral intercellular space is low (Boulpaep, Sackin 1980; Nagel et al. 1983). This underestimation is increased substantially if LIS is collapsed. A corresponding underestimation is done, if adequate compensation for the subepithelial tissue resistance or the fluid resistance is not done properly. These errors can be calculated with the simple distributed model of LIS using formulas, which can easily be deduced from the appendix of (Kottra, Frömter 1984b). Fig 5.7.1 shows results from such calculations. The problem of the subepithelial tissue resistance and the altering fluid resistance can be eliminated by measuring the transepithelial impedance and extrapolating the high frequency intersection point with the real axis in a Nyquist plot (Kottra, Frömter 1990a). The case of LIS resistance is more complicated, but if R_t increases simultaneously with decreasing R_a/R_b, it could be a sign of collapsing LIS and the results obtained by the 2D-cable analysis should be interpreted with caution.

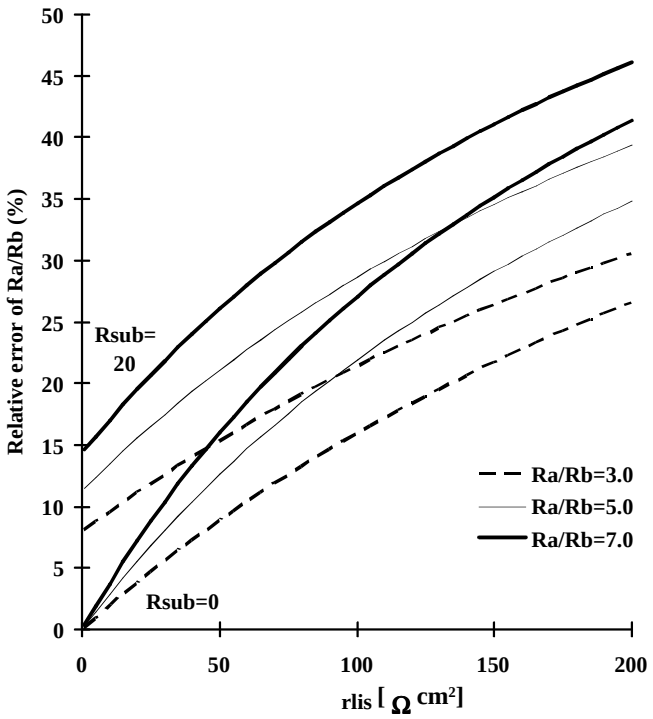

Fig 5.7.1 The relative error of R_a/R_b. The effect of increasing the resistance of lateral intracellular space (LIS) or subepithelial tissue resistance (R_{sub}) on the relative error of R_a/R_b are shown in the figure (R_b=3.0 kΩ·cm^2, ratio of lateral to basal membrane area =20, tight junction resistance = 1.0 kΩ·cm^2). The error is calculated as 100*(a_{true}-$a_{measured}$)/$a_{measured}$, where a_{true} is the correct value of R_a/R_b and $a_{measured}$ is the measured value of R_a/R_b.

5.8 Comparing the results of 2D-cable analysis and amiloride exposure technique (II)

In this series of experiments the basal intraepithelial resistances were determined with the 2D-cable analysis and the values were compared with those obtained by means of the amiloride exposure technique in same seven tissues. The cable analysis gave almost equal values (R_a= 16.3 ± 1.8 kΩ·cm^2, R_b =5.3 ± 0.9 kΩ·cm^2 and R_s= 915 ± 137 Ω·cm^2, N=7) as the amiloride exposure technique (R_a= 15.1 ± 1.2 k Ω·cm^2, R_b= 5.1 ± 0.8 kΩ·cm^2 and R_s= 921 ± 148 Ω·cm^2, N=7) (Fig 5.8.1). Under the following tolerance limits for the difference (2D-cable analysis - amiloride method) in each parameter ((-1.0 - 3.4) kΩ·cm^2, (-0.5 - 0.9) kΩ·cm^2 and (-54 - 42)

$\Omega \cdot cm^2$ for R_a, R_b and R_s respectively), these two methods can be regarded to be equivalent (p=0.05). The values obtained by the 2D-cable analysis during amiloride exposure in the same seven tissues were: $R_a = 45.2 \pm 9.3$ k$\Omega \cdot cm^2$, $R_b = 5.5 \pm 1.2$ k$\Omega \cdot cm^2$ and $R_s = 900 \pm 136$ $\Omega \cdot cm^2$. The R_a changed significantly ($p<0.02$, N=7) when compared to the basal values obtained by the same method, whereas the other resistances remained relatively stable.

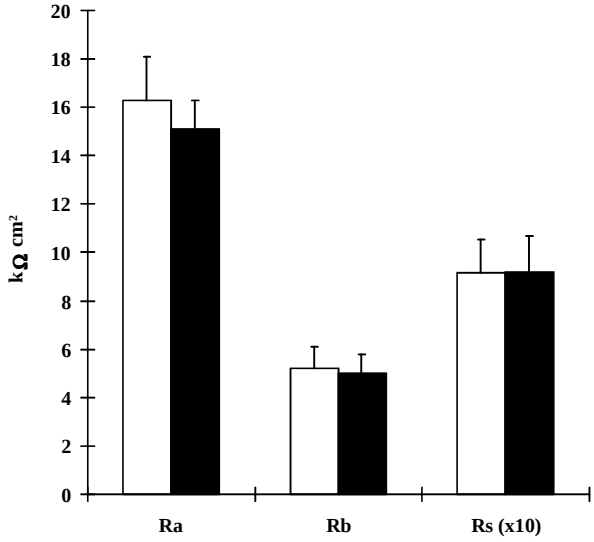

Fig 5.8.1 Comparison of methods. Comparison of 2D-cable measurement with the amiloride exposure technique in the same tissues. (White= calculated with 2D-cable analysis, Black= calculated with amiloride exposure technique in the same epithelia, Error bars = Standard error of mean, N=7)

5.9 Effect of luminal acid on epithelial parameters (III)

Intraepithelial resistances. During luminal exposure to the standard Ringer's solution (pH 7.25) the following values for the apical cell membrane, basolateral cell membrane and the shunt pathway resistances, respectively, were obtained with 2-dimensional cable analysis: 18.9 ± 1.3 k$\Omega \cdot cm^2$, 4.8 ± 0.5 k$\Omega \cdot cm^2$, 863 ± 81 $\Omega \cdot cm^2$ (N=24).

As illustrated in Fig 5.9.1, exposure to luminal pH 4.0 caused a slight but significant decrease in the apical cell membrane resistance (from 21.3 ± 2.6 k$\Omega \cdot cm^2$ to 18.5 ± 3.0 k$\Omega \cdot cm^2$, $p<0.05$, N=8), which

was restored at luminal pH 3.5 (from 18.5 ± 3.0 kΩ·cm^2 to 24.1 ± 3.9 kΩ·cm^2, p<0.05). The other intraepithelial resistances remained unchanged during this period (R_b= 4.3 ± 0.5 kΩ·cm^2, R_s= 824 ± 98 Ω·cm^2 for luminal pH 4.0).

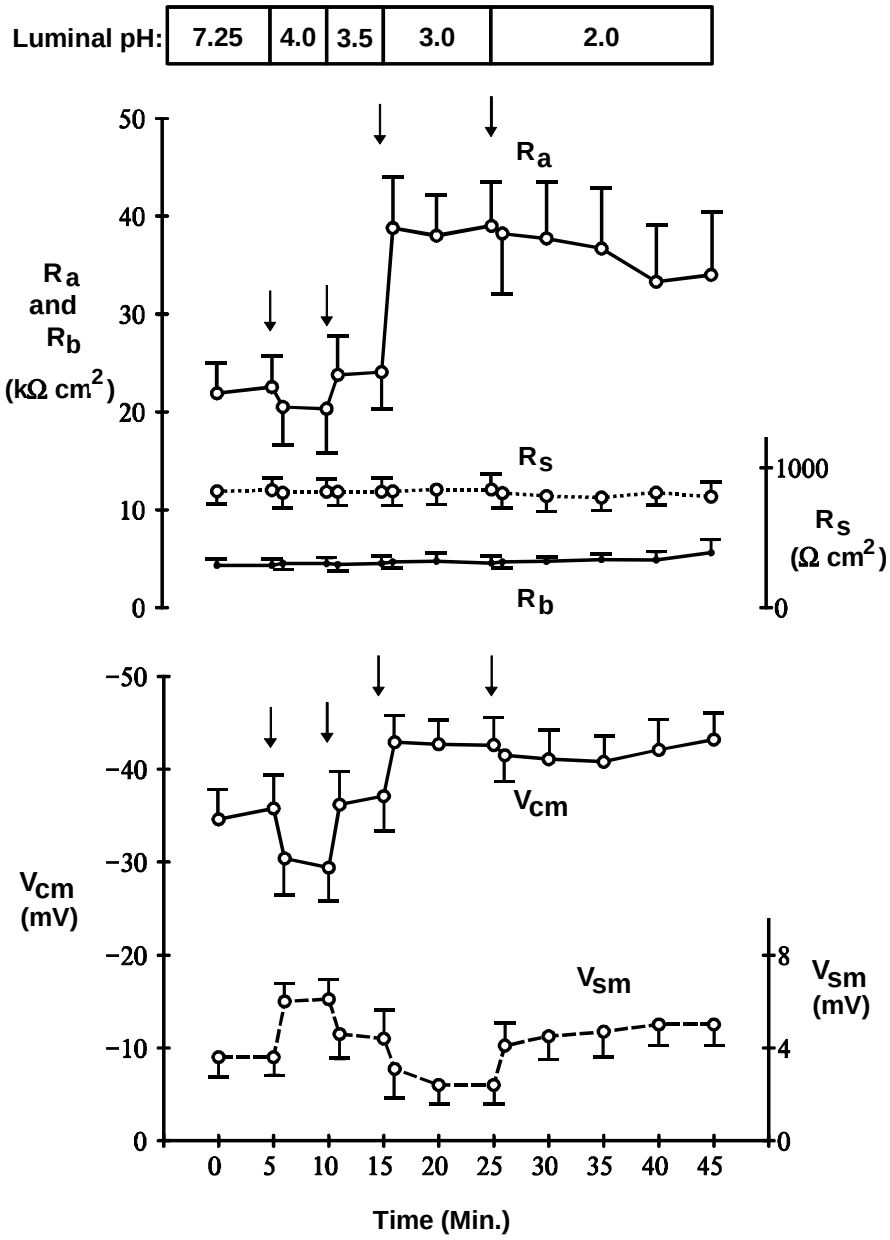

Figure 5.9.1 Effect of luminal acid on intraepithelial resistances and electric potentials (V_{cm}=apical cell membrane potential and V_{sm}=transepithelial potential, N=8).

During subsequent exposure to luminal pH 3.0 the apical cell membrane resistance increased suddenly from 24.1 ± 3.9 kΩ·cm^2 to 38.0 ± 2.3 kΩ·cm^2 (p<0.001), while the other measured resistances continued to remain unaffected (R_b= 4.7 ± 0.8 kΩ·cm^2, R_s= 844 ± 103 Ω·cm^2, N.S.).
During further luminal acidification to pH 2.0, the intraepithelial resistances first remained relatively stable (R_a= 37.7 ± 5.9 kΩ·cm2, R_b= 4.7 ± 0.5 kΩ·cm^2, R_s= 798 ± 102 Ω·cm^2.), but then the apical cell membrane resistance gradually decreased to 33.3 ± 5.9 kΩ·cm^2 (N.S. see Fig 5.9.1). The other measured resistances remained stable (R_b= 4.9 ± 0.8 kΩ·cm^2, R_s= 822 ± 93 Ω·cm^2).

Transmembrane potentials. During exposure to luminal pH 7.25, the apical cell membrane potential (V_{cm}) and the transmucosal potential (V_{sm}) were -35.1 ± 1.8 mV and +3.3 ± 0.4 mV, respectively (N=24).

Exposure to luminal pH 4.0 depolarised V_{cm} from -35.8 ± 3.7 mV to -29.4 ± 3.7 mV (p<0.01, N=8) and V_{sm} from 3.6 ± 0.7 mV to 6.1 ± 0.9 mV (p<0.01), but the changes were restored during exposure to luminal pH 3.5 (V_{cm} from -29.4 ± 3.7 mV to -36.7 ± 3.6 mV, p<0.01 and V_{sm} from 6.1 ± 0.9 mV to 4.4 ± 1.3 mV, p<0.05).

Subsequent luminal exposure to pH 3.0, V_{cm} was hyperpolarized from -36.7 ± 3.6 mV to -44.3 ± 2.6 mV (p<0.01) and V_{sm} from 4.4 ± 1.3 mV to 2.4 ± 0.8 mV (p<0.01), and V_{cm} remained fairly stable (from -44.3 ± 2.6 mV to -41.1 ± 3.3 mV, N.S.), and V_{sm} increased from 2.4 ± 0.8 mV to 4.5 ± 1.0 mV (p<0.05) during further luminal acidification to pH 2.0.

That the above changes were not due to increased Cl^- in acidic pH solutions was ruled out by a series of experiments in which the solutions were titrated with methanesulfonic acid instead of HCl (data not shown).

5.10 Membrane resistances, potentials and intracellular pH during exposure to luminal acid (III).

In this series of experiments the intracellular pH and the membrane resistances (the 2D-cable analysis) were measured simultaneously. The apical cell membrane resistance decreased slightly (from 25.6 ± 3.0 kΩ·cm^2 to 21.4 ± 4.1 kΩ·cm^2, p<0.02, N=6) and V_{cm} depolarized (from -34.4 ± 1.7

to -29.5 ± 3.0 mV, p<0.01) when the pH of the luminal solution was acidified from pH 7.25 to pH 4.0, while the intracellular pH remained relatively stable (pH_i from 7.35 ± 0.06 to 7.32 ± 0.07, N.S., Fig 5.10.1). The subsequent increase in the apical cell membrane resistance (from 21.4 ± 4.1 kΩ·cm^2 to 51.2 ± 4.3 kΩ·cm^2, p<0.02) and the hyperpolarization of V_{cm} (from -29.5 ± 3.0 mV to -41.8 ± 2.0 mV, p<0.02) induced by exposure to luminal pH 3.0 were associated with a slight but significant decrease in pH_i (from 7.32 ± 0.07 to 7.23 ± 0.06, p<0.04; N=6). During the following 10 minutes the intracellular pH recovered from 7.23 ± 0.06 to 7.28 ± 0.08 (N.S.) and was statistically indistinguishable from the value during exposure to luminal pH 4.0.

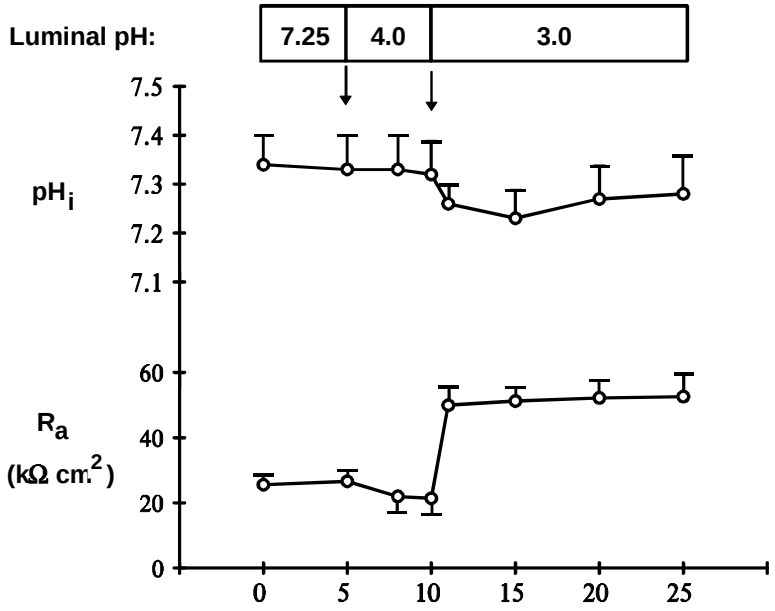

Figure 5.10.1 Effect of luminal acid on intracellular pH and R_a (N=6).

An example of pH_i measurement during luminal acidification is shown in Fig 5.10.2, which discloses that the pH_i decline occurs first, and hyperpolarization of the apical cell membrane potential occurs during the recovery period of pH_i. A similar temporal relationship was observed in all experiments of this type.

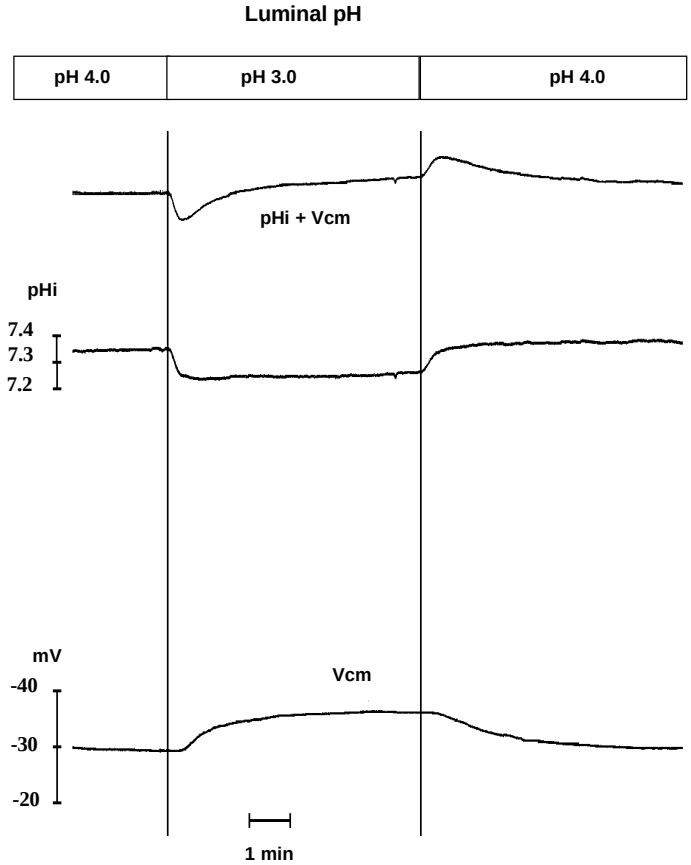

Fig 5.10.2 An example of intracellular pH (pHi) recording with luminal pH changing from pH 4.0 to 3.0. Pen offset compensation was used to show the accurate timing of changes.

5.11 Effect of substituting Na^+ for all luminal cations (III)

Intraepithelial resistances. In order to discover which ions were involved in the increase of R_a (and hyperpolarization of V_{cm}) due to luminal acid, ion-substitution experiments were performed. In this series of experiments the luminal side was first exposed to the standard Ringer's solution and thereafter to solutions in which Na^+ substituted for all the cations and Cl^- for all the anions at pH 4.0, pH 3.5 and pH 3.0. The serosal side was always perfused with the standard Ringer's solution. Under control conditions when both sides were perfused with the standard Ringer's solution, the following resistances were obtained: $R_a = 16.7 \pm 2.3$ kΩ·cm^2, $R_b = 4.0 \pm 1.2$ kΩ·cm^2 and $R_s = 505 \pm 29$ kΩ·cm^2 (N=5)(Fig 5.11.1).

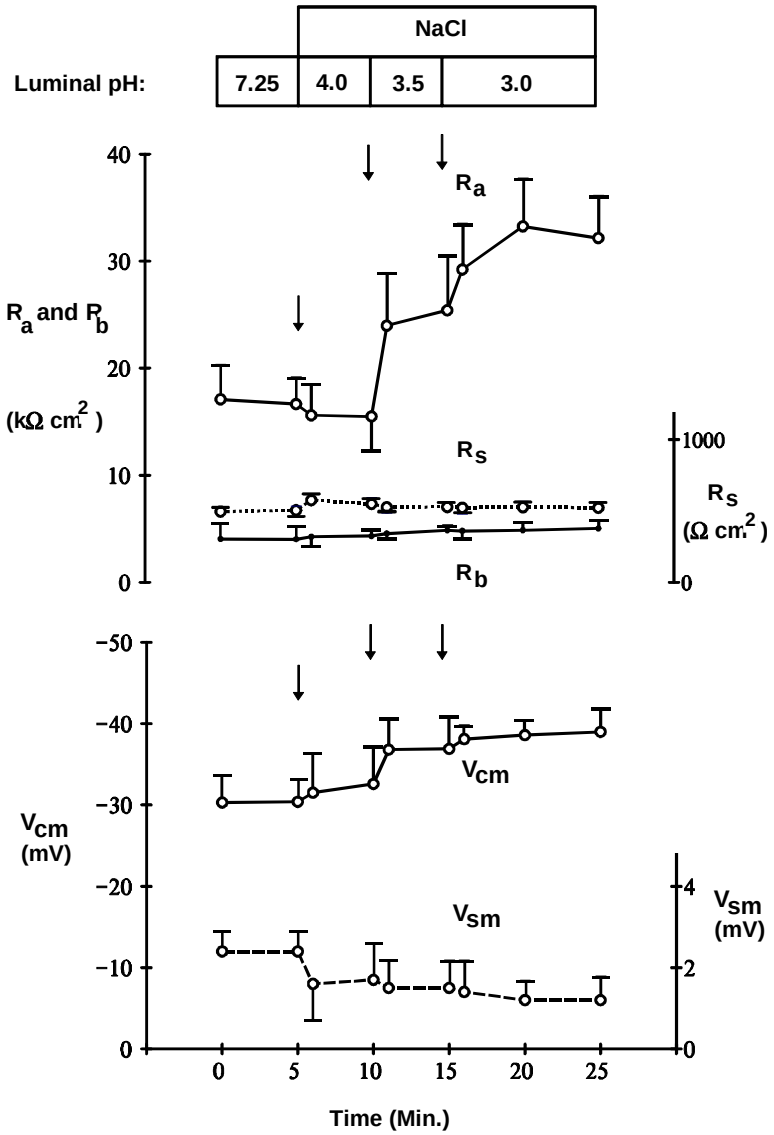

Figure 5.11.1 Effect of substitution of Na^+ for all luminal cations and Cl^- for all anions on intraepithelial resistances (R_a,R_b and R_s) and electric potentials (V_{cm} and V_{sm}) (N=5).

Exposure to luminal NaCl at pH 4.0 did not change the intraepithelial resistances significantly, although R_a tended to decrease slightly. Exposure to luminal NaCl at pH 3.5 increased the apical cell membrane resistance from 15.5 ± 3.3 kΩ·cm^2 to 25.4 ± 5.2 kΩ·cm^2 ($p<0.03$), while the other intraepithelial resistances remained relatively unaffected. Further acidification to luminal NaCl at pH 3.0 increased R_a from 25.4 ± 5.2 kΩ·cm^2 to 33.3 ± 3.7 kΩ·cm^2 ($p<0.05$), while the other resistances remained unchanged.

Transmembrane potentials. During luminal exposure to the standard Ringer's solution at pH 7.25 the apical cell membrane potential (V_{cm}) and the transmucosal potential (V_{sm}) were -30.4 ± 2.8 mV and

2.4 ± 0.5 mV, respectively (N=5). Exposure to luminal NaCl at pH 4.0 did not significantly change V_{cm}. Exposure to luminal NaCl at pH 3.5 hyperpolarized V_{cm} from -32.6 ± 4.7 mV to -36.9 ± 4.0 mV ($p<0.04$), but further acidification to luminal NaCl at pH 3.0 did not change V_{cm} significantly. Exposures to luminal pH 4.0, pH 3.5 and pH 3.0 (NaCl) did not change V_{sm} significantly.

5.12 Effect of substituting NMDG for all luminal cations (III)

Intraepithelial resistances. In this series of experiments the luminal side was first exposed to the standard Ringer's solution and thereafter to solutions in which Na^+ was substituted for all the cations and Cl^- for all the anions at pH 4.0, and thereafter to solutions in which $NMDG^+$ was substituted for all the cations and Cl^- for all the anions at pH 4.0, pH 3.5, and pH 3.0. The basolateral side was always perfused with the standard Ringer's solution. Under basal conditions when both sides were perfused with standard Ringer's, the following values were obtained: R_a= 17.1 ± 3.3 kΩ·cm^2, R_b= 4.0 ± 1.5 kΩ·cm^2 and R_s= 496 ± 32 kΩ·cm^2 (N=5).

Luminal exposure to NaCl at pH 4.0 did not change the intraepithelial resistances significantly (R_a= 15.6 ± 2.5 kΩ·cm^2, R_b= 3.9 ± 0.5 kΩ·cm^2, R_s= 533 ± 18 Ω·cm^2, N.S.).

Exposure to luminal NMDG-Cl at the same pH (pH 4.0) increased R_a from 15.6 ± 2.5 kΩ·cm^2 to 31.1 ± 2.3 kΩ·cm^2 ($p<0.01$) and R_s from 533 ± 18 Ω·cm^2 to 699 ± 43 Ω·cm^2 ($p<0.01$), but R_b remained stable (from 3.9 ± 0.5 kΩ·cm^2 to 3.6 ± 0.7 kΩ·cm^2, N.S.). Subsequent exposure to luminal NMDG-Cl at pH 3.5 or pH 3.0 did not change the intraepithelial resistances.

In the following, the relative changes are compared when the luminal solution is changed from Ringer's pH 7.25 either to Ringer's, NaCl, or NMDG-Cl solutions at the same pH. The relative change in R_a was significantly different for NMDG-Cl pH 3.5 solution (76.0 ± 18.8 %) when compared with that of Ringer's pH 3.5 (11.7 ± 6.6 %, $p<0.01$), but not when compared with NaCl pH 3.5 solution. No significant difference was seen with pH 3.0 solutions.

Transmembrane potentials. During luminal exposure to pH 7.25, the apical cell membrane potential (V_{cm}) and the transmucosal potential (V_{sm}) were -30.3 ± 3.4 mV and 2.4 ± 0.5 mV, respectively (N=5). Exposure to luminal NaCl at pH 4.0 did not significantly change V_{cm} or V_{sm}. However,

exposure to luminal NMDG-Cl at pH 4.0 momentarily hyperpolarized both V_{cm} (from -32.2 ± 4.9 mV to -47.9 ± 1.0 mV ($p<0.02$)) and V_{sm} (from 2.2 ± 1.1 mV to -4.7 ± 0.5 mV ($p<0.05$). Further exposure to luminal NMDG-Cl at pH 3.5 or pH 3.0, did not significantly change V_{cm} or $V_{sm.}$

5.13 Effect of intracellular acidification (III)

To explore whether the increase in R_a (and V_{cm}) due to luminal acidification was caused primarily by luminal acid, or whether it was secondarily mediated by the ensuing acidification of pH_i, a series of experiments were performed. In this series, an artificial intracellular acidification was provoked either by a basolateral 20mM NH_4^+ prepulse technique or by exposing the basolateral side to pH 6.8-7.0. The value of R_a/R_b was measured when an approximately 0.1 pH-unit decline was observed in intracellular pH [from 7.30 ± 0.05 to 7.19 ± 0.04 for the NH_4^+ group ($p<0.01$;N=8) and from 7.34 ± 0.03 to 7.22 ± 0.04 for the serosal acid group ($p<0.01$; N=11)].

In the NH_4^+ prepulse group, R_a/R_b decreased significantly from 3.11 ± 0.22 to 2.50 ± 0.18 ($p=0.01$), whereas in the apical cell membrane potential no significant change was observed (from -32.0 ± 5.8 mV to -29.0 ± 6.4 mV; N.S.). (The mucosal side was perfused with the Ringer's solution.)

Likewise, the serosal acid exposure group showed no significant change in R_a/R_b (from 3.08 ± 0.40 to 2.73 ± 0.37, N.S.), but a significant depolarization of V_{cm} (from -30.1 ± 3.2 mV to -25.0 ± 3.3 mV, $p=0.02$). (The mucosal side was perfused with MES buffered Ringer's pH 6.0 solution.)

5.14 Measurement of a_{Na}^{i} near the transition point (III)

These above findings suggest that the increased R_a following exposure to luminal acid is due to the closure of sodium-permeable channels in the apical membrane. If so, this should have an effect on intracellular sodium activity when the luminal pH is decreasing close to the transition point. In this series of experiments a_{Na}^{i} was recorded with single-barrelled ion-selective electrodes. Luminal acid was changed from pH 4.0 to pH 3.0 in normal Ringer's solutions to induce the resistance transition in the apical cell membrane. The shift observed in the R_a/R_b-ratio was parallel to a reversible change in a_{Na}^{i} from 8.1 ± 0.6 mM to 6.3 ± 0.6 mM (N=9; p<0.01, Fig 5.14.1).

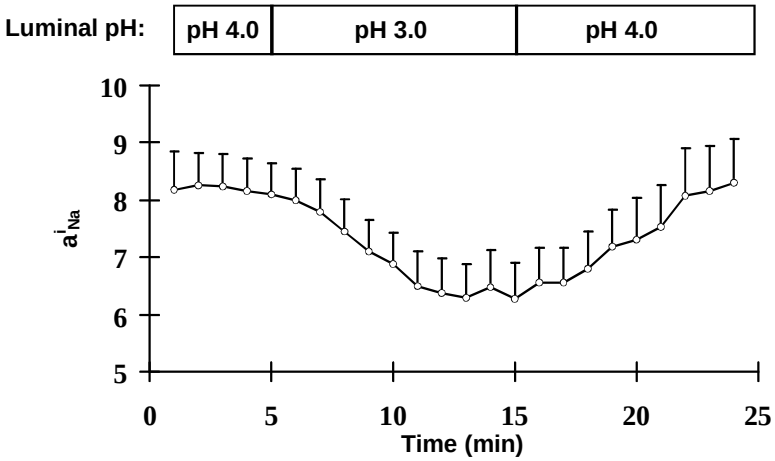

Figure 5.14.1 Effect of luminal acid on intracellular Na^+ activity (N=9).

5.15 Effect of amiloride during luminal acid (III)

The effect of amiloride in the presence of luminal acid was investigated at two pH levels, pH 4.0 and pH 3.0. The basal values with luminal pH 7.25 were 4.38 ± 1.12 for R_a/R_b and -41.1 ± 5.0 mV for V_{cm}. At luminal pH 4.0, amiloride increased R_a/R_b from 4.26 ± 1.21 to 9.08 ± 0.80 (p<0.01; N=5). In contrast, at pH 3.0 (where R_a/R_b is already elevated), amiloride caused no further increase in R_a/R_b (from 7.80 ± 0.82 to 7.74 ± 0.84, N.S., N=5). At luminal pH 4.0 amiloride hyperpolarized V_{cm} from -36.5 ± 7.4 mV to -55.9 ± 5.4 mV (p<0.05), but caused no further changes in V_{cm} at luminal pH 3.0 (from -53.2 ± 3.0 mV to -53.5 ± 3.7 mV, N.S.). During the change in the luminal pH

from pH 4.0 to pH 3.0, R_a/R_b increased from 4.84 ± 1.18 to 7.80 ± 0.82 ($p<0.05$), and the V_{cm} hyperpolarized from -44.1 ± 3.0 mV to -53.2 ± 3.0 mV, ($p<0.05$), as usual.

In a second series of experiments, the epithelium was exposed continuously to 0.1 mM amiloride. Adding amiloride to luminal pH 7.3 increased R_a/R_b (from 3.81 ± 0.51 to 6.98 ± 0.50, p=0.01) and hyperpolarized V_{cm} (from -25.8 ± 1.1 mV to -34.2 ± 1.5 mV, $p<0.05$), as usual. During continuous exposure to 0.1mM luminal amiloride (when R_a/R_b and V_{cm} are already elevated), acidification of luminal pH from pH 7.3 to pH 3.0 caused neither further increase in R_a/R_b (from 6.98 ± 0.5 to 6.64 ± 0.58, N.S.; N=7) nor any hyperpolarization of V_{cm} (from -34.2 ± 1.5 mV to -32.9 ± 1.5 mV N.S.).

5.16 Effects of increasing concentrations of luminal ethanol (IV)

In this series of experiments luminal ethanol was step-wise (with 5% steps, vol/vol) increased from 0% to 15% at luminal pH 3.0 and cell membrane resistances were measured using the 2D-cable analysis. The possible adaptation was not examined. The findings show (Fig 5.16.1) that following exposure to luminal 5% ethanol the initial effect is a decrease in basolateral cell membrane resistance (from 5.5±0.8 to 4.1±0.5 kΩ·cm^2, $p<0.05$, N=18) and hyperpolarization of the apical cell membrane potential (V_{cm}) (from –36.5±1.4 to –45.8±2.8 mV, $p<0.05$, N=18). Later (at 20 minutes), also the apical cell membrane resistance is slightly decreased (from 29.4±3.8 to 25.9±4.1 kΩ·cm^2, $p<0.05$). In most experiments (11 out of 18) V_{cm} started to depolarize after the initial hyperpolarization promoted by 5% ethanol exposure, but this depolarization was not statistically significant. Exposure to luminal 10% ethanol caused further decrease in R_a and R_b, increased the internal resistance (R_x), and also increased transmucosal potential (V_{sm}). At the beginning of the 10% ethanol exposure also V_{cm} was hyperpolarized. Exposure to 15% ethanol induced a profound decrease in R_a, a smaller decrease in R_b, a decrease in the shunt resistance (R_s), depolarization of V_{cm} and an increase in V_{sm}. Taken all together, these changes probably indicate a major damage to the epithelia.

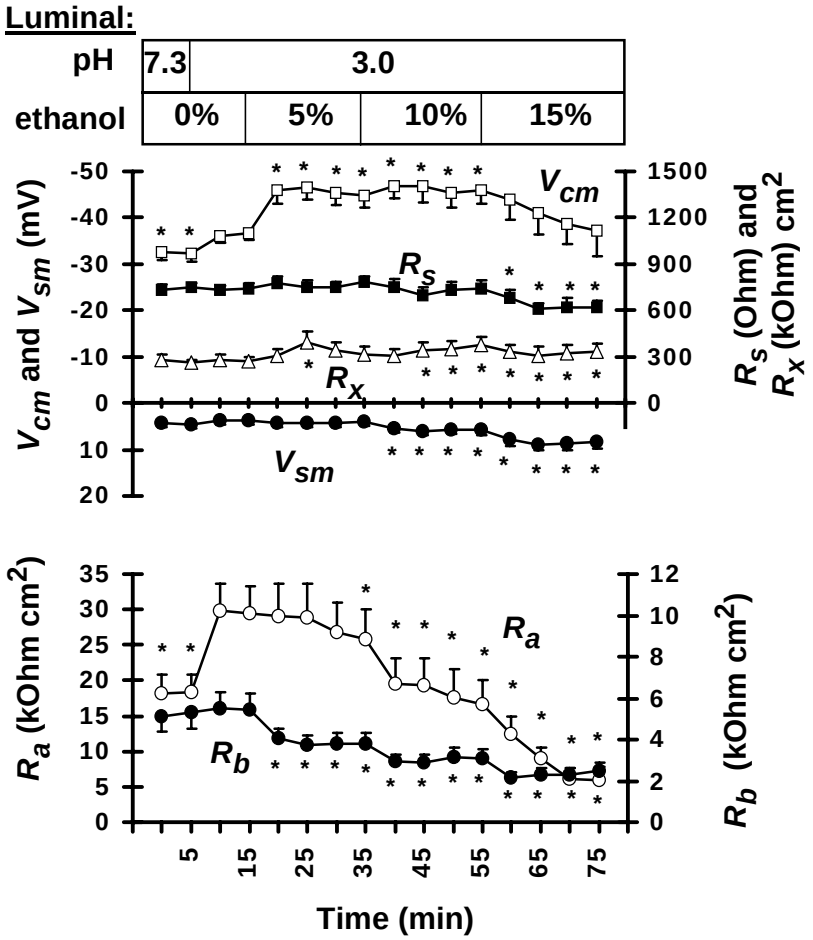

Fig 5.16.1 The effect of luminal ethanol (ETOH) on apical (R_a) and basolateral (R_b) cell membrane resistances, shunt resistance (R_s), internal resistance (R_x) and on apical (V_{cm}) and transmucosal (V_{sm}) potentials. * (or † in the case of R_s) indicate significant ($p<0.05$) differences as compared to luminal exposure to 0% ethanol at pH 3.0 (N=18). As shown before, the sudden increase in R_a and hyperpolarization of V_{cm} following luminal pH 3.0 exposure are due to closure of amiloride sensitive epithelial Na^+ channel on the apical cell membrane (Study III).

Luminal amiloride (0.1 mM) was able to prevent the decrease of R_a after 20 minutes exposure to 5% or 10% luminal ethanol ((from 28.5±6.9 to 30.3±6.6 (5% ethanol) and to 24.7±4.3 (10% ethanol) kΩ·cm^2, N.S., N=8), but not during stronger ethanol exposure (9.7±4.8 kΩ·cm^2 after 20 minutes exposure 15% luminal ethanol, $p<0.05$).

5.17 Effect of blocking of the basolateral K^+-channel (IV)

The above experiments suggest that the primary target of luminal ethanol in the gastric epithelium is the basolateral cell membrane, where it decreases membrane resistance (R_b). The

following experiments were designed to further elucidate these effects. In this series of experiments blockers of K^+ channels were applied on to the serosal side of the mucosa. Serosal quinine (1 mM) had an expected effect on membrane parameters, i.e. increase in R_b and depolarization of V_{cm}. As shown in figure 5.17.1 (N=7), serosal quinine was able to abolish, at least partly, the decrease in R_b as well as the hyperpolarization of V_{cm} promoted by 5% luminal ethanol. This suggests that luminal ethanol has an effect on basolateral potassium channel. During exposure to luminal ethanol R_a started to decline, but the decrease was not significant.

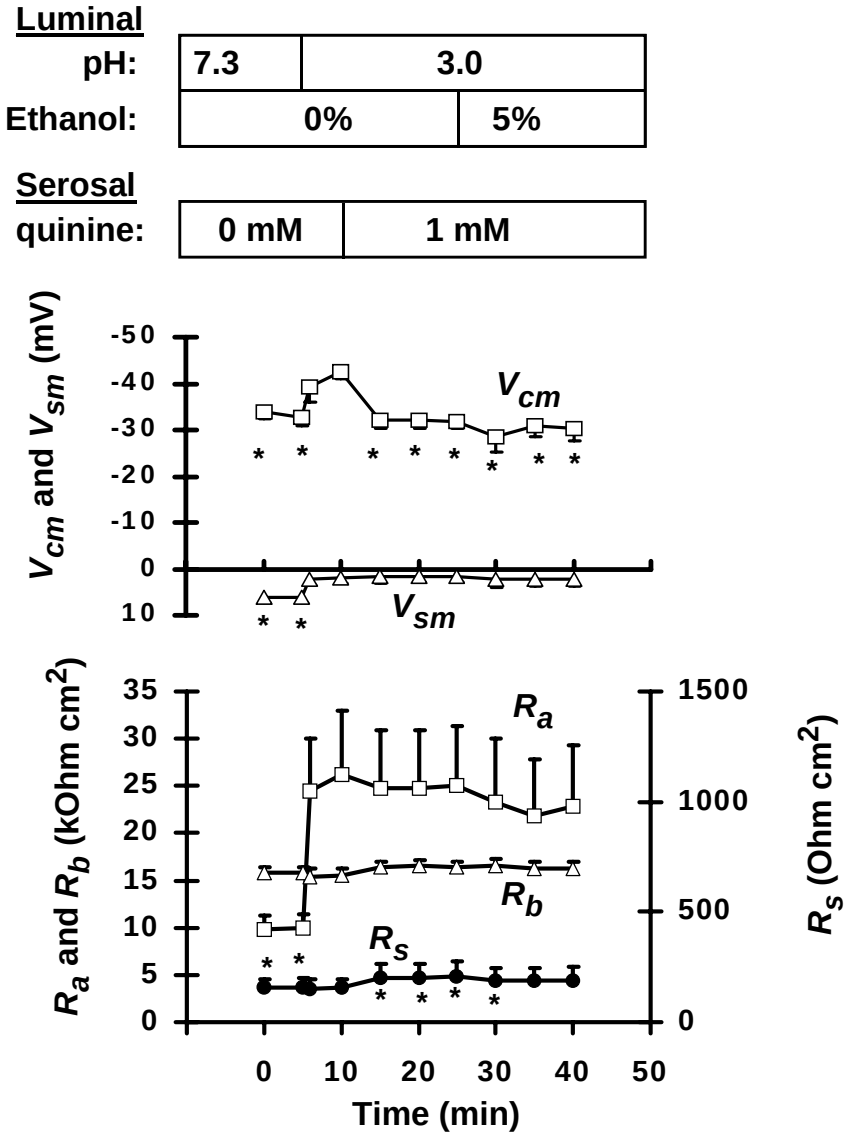

Fig 5.17.1 The effect of serosal quinine on luminal ethanol treatment. Serosal quinine was able to abolish the decrease in R_b and hyperpolarization in V_{cm} promoted by luminal ethanol. * indicates significant ($p<0.05$) differences as compared to luminal pH 3.0 (0% ethanol) exposure in the absence of serosal quinine (N=7). During quinine treatment luminal ethanol provoked no significant changes.

5.18 Effect of ethanol on relative K^+ conductance of the basolateral membrane (IV)

In order to further elucidate the role of basolateral K^+ channels in ethanol induced epithelial injury the effect of luminal ethanol on relative basolateral K^+ conductance was examined. In these experiments the changes in V_{cs} induced by increasing basolateral K^+ concentration from 4mM to 30mM were measured in the same cells before and during exposure to luminal 5% ethanol at pH 3.0. In the presence of luminal ethanol, the K^+ increment was applied after 5 minutes exposure to luminal ethanol. The results (Study IV) demonstrate that basolateral K^+ conductance is increased during luminal ethanol exposure, thus confirming the above results obtained by the 2D-cable analysis and K^+ channel blockers. An example of these experiments is shown in figure 5.18.1 Because similar changes could have been caused also by a large increase in the apical cell membrane resistance, the above measurements were repeated in a different series of experiments, where the mucosal solution was replaced by an NMDG-Cl containing solution at pH 3.0. This did not alter the results, which confirms that the V_{cm} hyperpolarization occurring almost instantly after luminal ethanol exposure is a process confined to the basolateral cell membrane.

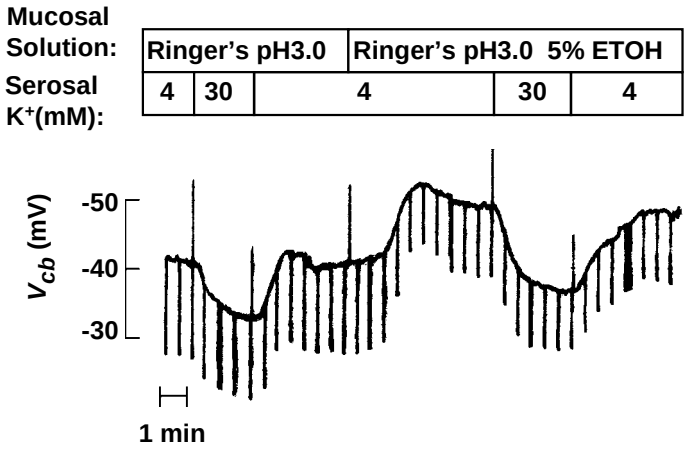

Fig 5.18.1 An example of an experiment demonstrating the effect of luminal ethanol on basolateral relative K^+ conductance. V_{cs} is the basolateral cell membrane potential. The upward deflections indicate solution changes

5.19 Effect of luminal ethanol on relative Na^+, K^+ and Cl^- conductances of the apical cell membrane (IV)

The effect of luminal ethanol on relative Na^+, K^+ and Cl^- conductances of the apical cell membrane were investigated by ion concentration step experiments. The changes in V_{cm} induced by decreasing mucosal Na^+ concentration from 105 mM to 50 mM and thereafter increasing mucosal K^+ concentration from 4 to 54 mM were measured in the same cells before and during exposure to luminal 5% ethanol at pH 3.0. Similar experiments were performed by changing luminal Cl^- concentration form 89 to 9 mM. The results show that all these conductances are increased slightly (Study IV). Experiments were performed also with higher luminal ethanol concentrations (10% and 15%). With 10% ethanol the changes of ΔV_{cm} due to Na^+, K^+ and Cl^- steps were not significantly higher (9.0±1.8 mV, -4.7±1.9 mV and -7.2±0.6 mV for Na^+, K^+ and Cl^-, respectively) than in connection with 5% ethanol. The results with 15% ethanol are somewhat unreliable due to a large drift in V_{cm} (data not shown). The increase in ΔV_{cm} promoted by Na^+ steps is more prominent at luminal pH 4.0. This increase is blocked by luminal amiloride, suggesting a protein-coupled effect of ethanol on apical membrane rather than membrane fluidization. Luminal Cl^- channel blockers NPPB (0.1mM, N=5) or 9-AC (1mM, N=5) did not reduce ΔV_{cm} caused by luminal Cl^- steps during luminal 5% ethanol exposure (data not shown).

5.20 Effect of luminal ethanol on cell volume (IV)

The ethanol concentrations (5%, 10% and 15% vol/vol) used in the above experiments are strongly hyperosmolar, corresponding molar concentrations of 0.86, 1.71 and 2.57 mol/L of ethanol, respectively. Therefore, luminal exposure to ethanol might also influence epithelial cell volume. Further, K^+ channels together with Cl^- transport are generally involved in cell volume regulation. Therefore changes in cell volume were measured using TMA as an intracellular volume indicator. Following exposure to luminal 5% ethanol, cell volume decreased by -16±4% (N=10, p=0.006) in 5 minutes. This shrinkage was reduced to -2±4% (N=7, p=0.03, Fig 5.14.1) in the presence of serosal quinine (1 mM, Fig 5.20.1). After 5 minutes exposure to 10% luminal ethanol the respective values were -30±9% and -5±14%. If the measurements were continued with higher luminal ethanol concentrations, the indicator tended to leak out in some experiments, suggesting a perturbation of the integrity of the apical cell membrane. Further evidence of the

basolateral potassium channel involvement in cell volume changes during luminal ethanol exposure was sought by temporally changing the luminal potassium concentration from 4 mM to 30 mM before and after exposure to luminal 5% ethanol and measuring changes in cell volume. During the first two minutes after serosal potassium concentration change the volume changed 17±6% and 27±7% (N=5, p=0.03) with or without 5% luminal ethanol, respectively.

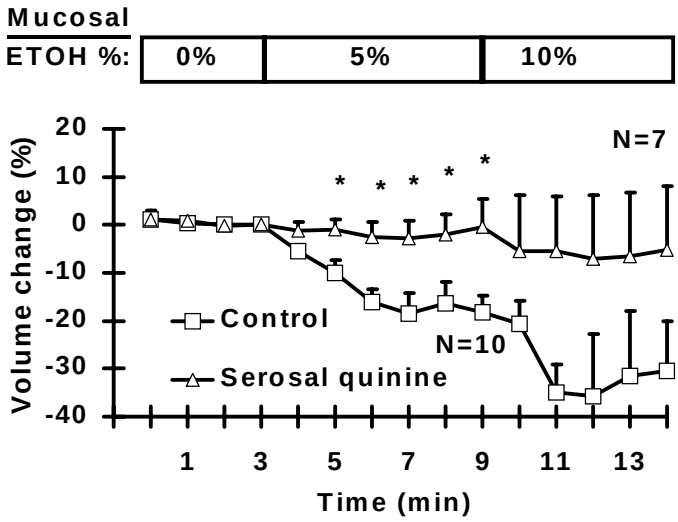

Fig 5.20.1 A. Luminal ethanol decreases cell volume. This volume decrease is partially inhibited by serosal potassium channel blocker, quinine (1mM). * $p<0.05$ as compared to control group.

6. DISCUSSION

The specific aim of this study was to establish a reliable and temporally fast method to measure cell membrane and shunt resistances in simple epithelia and use this technique to measure membrane resistances in the gastric antrum during luminal exposure to acid and ulcerative agents. In order to be temporally fast the method should not require any solution changes or added inhibitors. The requirement of such a method was already evident during study (I), where the effect of three barrier breaking agents on intracellular pH and epithelial resistances were examined. In this study amiloride, a sodium channel inhibitor, was used to change apical cell membrane resistance, in order to calculate apical, basolateral and shunt pathway resistances. This method does not function reliably at acidic pH and therefore its use is restricted in our studies. In the second study (II) intraepithelial two dimensional cable analysis was improved by using multiple electrodes simultaneously and by sequentially applying the intraepithelial current through different electrodes thus taking advantage of their spatial relationship. In the third and fourth studies (III, IV) the technique developed in II were applied to investigate the effects of luminal acid and luminal ethanol on epithelial resistances of the gastric antrum.

The necturus antrum used in these studies is a flat epithelium with well conducting gap junctions. It has also relatively large cells, which are easy to impale with electrodes, and therefore it is frequently used as a model in epithelial studies involving microelectrode technique. Necturus stomach has three distinctive areas, i.e. corpus, fundus and antrum, as in humans. Acid and pepsinogens are produced in the oxyntopeptic cells, whereas in humans there are two different cell types for this purpose, namely parietal and chief cells.

The basal values of R_a obtained in the study II-IV are higher than those obtained in previous studies (Ashley et al. 1985), but R_b agreed well. There may be many methodological reasons for these differences, such as in feeding of the animals, the keeping up conditions of the animals or systematic differences in electrodes and impalements. If the *Necturi* were fasted for longer periods or if they were not healthy, the R_a/R_b tended to be lower. In rabbit urinary bladder epithelium diet has an effect on permeability ratios (P_{na}/P_k) of the epithelial amiloride-sensitive channel (Lewis, de Moura 1982). In study II the intraepithelial two-dimensional method was validated for *Necturus* gastric antrum by measuring epithelial resistances both with the amiloride

technique and with the intraepithelial two dimensional cable analysis. The values obtained with these two techniques were found to be near each other in the same tissues. It was also found in practise that an incorrect distance configuration could ruin the precision of the measurement. It was deduced that using distance configurations similar to those in fig. 5.5.3 with adaptation to individual experiments, would probably be preferable in practise.

In study I, luminal acid (pH 3.0) had a small acidifying effect on intracellular pH and an increase in R_a/R_b and R_t. The increase in R_a/R_b due to luminal acid has been previously shown (Kivilaakso, Kiviluoto 1988) and it is sodium dependent (Rutten et al. 1989). Whether the increase in R_a/R_b was caused by increase in R_a or decrease in R_b could not be deduced from the data of the study I. In study III the improved intraepithelial 2D cable analysis showed that the increase in R_a/R_b provoked by luminal acid is due to an increase in R_a. Further, it was shown that this increase in apical cell membrane resistance was due to closure of epithelial amiloride sensitive sodium channel. The finding that during continuous amiloride exposure the effects of luminal acid on R_a/R_b and V_{cm} are abolished (III) suggests that the effects of amiloride and luminal acid are mediated by closing the same channel. This will also explain, why the amiloride technique was not a reliable measurement method for epithelial resistances during luminal acid exposure. During luminal acid the amiloride sensitive channels will be at least partially closed and luminal amiloride would cause only very minor changes in the R_a, thereby invalidating the precision of the method.

Changing luminal pH from 4.0 to 3.0 induced an increase in R_a in the presence of plain NaCl solution, but not in the presence of plain NMDG-Cl solution (III), presumably because the oversized NMDG could not permeate through sodium channels. This is an evidence for involvement of sodium channels in the increase of R_a caused by luminal acid (ph 3.0). After lowering the luminal pH from pH 4.0 to pH 3.0, there is a small decrease in intracellular pH_i associated with an increase in apical cell membrane resistance and a hyperpolarization of apical cell membrane potential followed by a small decrease in intracellular sodium activity. The intracellular acidification actually precedes the membrane resistance and cell membrane potential changes, which might indicate that protons act as a mediator for closure of these channels. This hypothesis was tested by induction of intracellular acidosis by NH_4^+ prepulse technique or with basolateral exposure to acid, but this did not induce apical cell membrane

potential hyperpolarization or increase in R_a/R_b. This suggests that luminal acid exerts its actions extracellularly from the luminal side of the apical cell membrane. It is possible that protons affect the channel molecules by protonating a few amino acid residues and thereby inducing conformational changes and closure of the pore. It has been shown with patch clamp experiments in rat cortical collecting tubule that the epithelial amiloride inhibitable sodium selective channels can be directly inhibited by protons (Palmer 1982), which supports the above presented hypothesis. This kind of blockade would also be very fast, because of the rapidity of protonation-deprotonation reactions (Hille 1984).

Taurocholate induced an immediate intracellular acidification and decrease in R_a/R_b and to a lesser degree in R_t (I). These findings suggest that taurocholate affects primarily the apical cell membrane conductance thereby increasing proton influx to the cytoplasm. With amiloride technique it was shown that after 5 minutes exposure to luminal 10 mM taurocholate the cellular resistances were decreased, but the shunt pathway resistance stayed relatively stable. The exact damaging of mechanisms of taurocholate to the cell membranes remains obscure, but it is generally believed to be related to the detergent properties of taurocholate. The epithelial damage of taurocholate in acidic conditions might be mediated by absorption and accumulation of protonated bile acids into the mucosa and increasing the apical cell membrane conductance (Duane et al. 1982). Bile acids have been shown to inhibit Na^+/K^+ ATPase activity (Little et al. 1977) thereby reducing the driving force of sodium needed by sodium dependent acid extrusion mechanisms.

Exposure of the *Necturus* antrum to acidified 10 mM luminal ASA induced initially an alkalisation of intracellular pH followed by acidification (I). R_t remained relatively stable during 10-15 minutes where after it started to decrease. In R_a/R_b there was an initial increase lasting for 6-9 minutes, whereafter it rapidly decreased followed by intracellular acidification. In apical cell membrane potential an initial hyperpolarization was seen followed by a more rapid depolarization. Cheung et al. (1985) also observed this hyperpolarization and increase in R_a/R_b, at neutral luminal pH, but not in acidic pH (pH 4.0). The reason for this discrepancy is not known, but it might be related with the different pH:s used pH 4.0 vs pH 3.0). Using amiloride

technique a significant increase in basolateral resistance was observed. These complex changes in the membrane parameters will require further work to be elucidated thoroughly.

Exposure to 20% luminal ethanol at pH 3.0 caused an immediate progressive decrease in R_t and a small transient hyperpolarization in V_{cm}. R_a/R_b started to decrease with a short delay followed by a decrease in intracellular pH. This suggests that the first effects of luminal 20% ethanol were the paracellular pathway and that the acidification of the cells were mediated by a direct damaging action of ethanol on the apical cell membranes. Ethanol also inhibits membrane bound ATPases thereby (Bailey et al. 1987) lowering the activity of sodium dependent acid extrusion mechanisms. Further studies with luminal ethanol showed that the first effects of 5% luminal ethanol were observed on the basolateral cell membrane, namely the opening of basolateral potassium channel (IV). In study IV the basolateral conductance of surface epithelial cells was observed to increase shortly after exposure to luminal 5% ethanol. The simultaneous hyperpolarization of V_{cm} could be explained with the opening of basolateral potassium channel. This hypothesis was tested with ion concentration step experiments and further by blocking basolateral potassium channel with quinine. Ion concentration step measurements showed that there was increased potassium conductance at the basolateral cell membrane. Basolateral quinine exposure inhibited the effect of luminal 5% ethanol on basolateral conductance change and changes in V_{cm}. Altogether these observations confirmed the hypothesis that luminal 5% ethanol induces increase in the basolateral potassium conductance. Ethanol is known to potentate the activation of Ca^{2+} activated K^+ channels in cell membranes (Chu et al. 1998) and ethanol is also known to increase cytosolic Ca^{2+} levels in human gastric cell line called AGS (Miller et al. 2001). Whether this is the mechanism that underlies the present findings, remains to be worked out. The observation that artificial increase of intracellular free calcium in Necturus antral mucosa causes similar effects (e.g. increase in R_a/R_b and hyperpolarization in V_{cm}) (Rutten, Moore 1991) as opening of basolateral K^+ channels is consistent with the hypothesis, that ethanol opens calcium activated K^+ channels. The hyperpolarization observed in study I could well arise from the opening of the basolateral potassium channel, but no increase was observed in R_a/R_b. This discrepancy might arise from the fact that in study I 20% ethanol was used instead of 5% (as used in study IV) and the increase in R_a/R_b remained unnoticed. After 5 minutes exposure to 20% luminal ethanol R_a, R_b and R_s were decreased. This is actually in accordance with study IV, where similar effects were seen with 15% luminal ethanol. During prolonged

exposure to luminal 5% ethanol also R_a decreased and this decrease was stronger with 10% and 15% ethanol. This decrease might arise from an increase in apical lipid membrane fluidity or even from a breakdown of the integrity of the apical cell membrane. The breakdown of the membrane might be the reason why our volume indicator tended to leak out from the cells during exposure to 15% luminal ethanol. It has been shown (with NMR) that as low as 1% ethanol concentration affects the phospholipids of rat gastric surface epithelial cells promoting a change in membrane fluidity (Bailey et al. 1987). Exposure to 6.25% ethanol promoted fluorescein to leak out from the surface mucus cells and mucous neck cells of rat gastric mucosa indicating damage of cell membranes (Sue, Guth 1985). It was further shown in study IV that the opening of basolateral potassium channel leads to cell volume decrease, which could also be inhibited with serosal quinine.

The aims of this study were reached relatively well. A reliable technique was developed for measuring epithelial cell membrane and shunt resistances. This technique, improved intraepithelial two dimensional cable analysis, was validated for *Necturus* antrum. Using this technique it was found that luminal acid closes apical sodium channels thereby preventing diffusion of protons in to the surface epithelial cells. The closing of apical sodium channels also contributes to the maintenance of sufficient transmembrane sodium gradient for sodium dependent acid equivalent transport extrusion across the basolateral cell membrane The first electrophysiological effects of luminal ethanol were shown to be the opening of basolateral potassium channel leading to cell volume shrinkage. These are obviously among the first functional perturbations that might precede and underlie ethanol induced gastric mucosal injury.

7. ACKNOWLEDGEMENTS

The present study was carried out at the Department of Surgery, the Division of Gastroenterology, University of Helsinki.

I have had the privilege to work under the supervision of Professor Eero Kivilaakso, the Head of the Department of Surgery in the University of Helsinki. His intelligence and skills in scientific work have provided me with continuous encouragement during this study. His contribution has been absolutely crucial for this study.

I am especially grateful to Docent Tuula Kiviluoto and Docent Pauli Puolakkainen for their endless enthusiasm and important advice and guidance in the world of medical science.

I express my warmest thanks to Ms Arja Vermasvuori for her endless support and interest in my work.

I owe my sincerest thanks to Mrs Paula Kokko for most excellent technical assistance during various phases of the laboratory work. She has also become a friend of mine, who owes the ability to think in scientific terms. I like to thank Ms Päivi Happo for her technical assistance and for creating nice and warm atmosphere in to our laboratory. My special thanks go to Mrs Merja Kirsi-Sihtola for joyful discussions about matters and states in the scientific world. She is always cheering up people who are lost in scientific mist.

I express my greatest gratitude to my wife Tuire, who has always encouraged and supported me during this study. In addition I am sincerely grateful to our children Elias, Emilia and Linnea for continuous enthusiasm and interest into my work.

Helsinki, 06 November 2003

Harri Mustonen

8. REFERENCES

Adams CL, Nelson WJ. Cytomechanics of cadherin-mediated cell-cell adhesion. *Current Opinion in Cell Biology* 10:572-77,1998.

Adorante JS. Regulatory volume decrease in frog retinal pigment epithelium. *Am J Physiol* 268:C89-C100,1995.

Alberts B, Johnson A, Lewis J, Raff M, Roberts K, Walter P. *Molecular Biology of the Cell*, 4th ed. New York: Garland Science, 2002.

Amman D. *Ion-Selective Microelectrodes; Principles, Design and Application*. Berlin: Springer-Verlag, 1986.

Angst BD, Marcozzi C, Magee AI. The cadherin superfamily: diversity in form and function. *Journal of Cell Science* 114:629-41,2001.

Arakawa T, Kobayashi K, Fukuda T, Higuchi K, Sakuma H, Kobayashi K. Early ultrastructural changes of surface epithelial cells isolated from rat gastric mucosa after exposure to ethanol with or without 16,16-dimethylprostaglandin E2. *J Clin Gastroenterol* 14 Suppl 1:S59-S63,1992.

Ashcroft FM. *Ion Channels and Desease*. San Diego: Academic Press, 2000.

Ashley SW, Soybel DI, De L, Cheung LY. Microelectrode studies of Necturus antral mucosa. II. Equivalent circuit analysis. *Am J Physiol* 248:G574-G579,1985.

Bailey RE, Levine RA, Nandi J et al. Effects of ethanol on gastric epithelial cell phospholipid dynamics and cellular function. *Am J Physiol* 252:G237-G243,1987.

Ballard HJ, Wilkes JM, Hirst BH. Effect of alcohols on gastric and small intestinal apical membrane integrity and fluidity. *Gut* 29:1648-55,1988.

Bates DM, Watts DG. Nonlinear Regression:Iterative Estimation and Linear Approximations. *Nonlinear Regression Analysis & It's applications.* New York: John Wiley & Sons 32-66, 1988.

Bevington PR. *Data Reduction and Error Analysis for the Physical Sciences*. McGraw-Hill, 1969.

Boulpaep EL, Sackin H. Electrical analysis of intraepithelial barriers. *Curr Top Membr Transport* 169-97,1980.

Cereijido M, Shoshani L, Contreras RG. Molecular physiology and pathophysiology of tight junctions. I. Biogenesis of tight junctions and epithelial polarity. *American Journal of Physiology - Gastrointestinal & Liver Physiology* 279:G477-G482,2000.

Chao P, Ammann D, Oesch U, Simon W, Lang F. Extra- and intracellular hydrogen ion-selective microelectrode based on neutral carriers with extended pH response range in acid media. *Pflugers Arch* 411:216-19,1988.

Chu B, Dopico AM, Lemos JR, Treistman SN. Ethanol potentiation of calcium-activated potassium channels reconstituted into planar lipid bilayers. *Mol Pharmacol* 54:397-406,1998.

Clausen C, Lewis SA, Diamond JM. Impedance analysis of a tight epithelium using a distributed resistance model. *Biophysical Journal* 26:291-317,1979.

Dinoso VPJ, Ming S, McNiff J. Ultrastructural changes of the canine gastric mucosa after topical application of graded concentrations of ethanol. *Am J Dig Dis* 21:626-32,1976.

Duane WC, Wiegand DM, Sievert CE. Bile acid and bile salt disrupt gastric mucosal barrier in the dog by different mechanisms. *American Journal of Physiology* 242:G95-G99,1982.

Flemström G. Gastric and Duodenal Mucosal Secretion of Bicarbonate. In Johnson LR, ed. *Physiology of the Gastrointestinal Tract.* New York: Raven Press 1285-309, 1994.

Forstner FF, Forstner GG. Gastrointestinal Mucus. In Johnson LR, ed. *Physiology of the Gastrointestinal Tract.* New York: Raven Press 1255-83, 1994.

Frömter E. The route of passive ion movement through the epithelium of Necturus gallbladder. *J Membr Biol* 8:259-301,1972.

Frömter E, Gebler B. Electrical properties of amphibian urinary bladder epithelia. III. The cell membrane resistances and the effect of amiloride. *Pflugers Archiv - European Journal of Physiology* 371:99-108,1977.

Hille B. *Ionic Channels of Excitable Membranes*, 1 ed. Sunderland: Sinauer Associates Inc., 1984.

Hirokawa M, Miura S, Yoshida H et al. Oxidative stress and mitochondrial damage precedes gastric mucosal cell death induced by ethanol administration. *Alcoholism, Clinical & Experimental Research* 22:111S-4S,1998.

Hirst BH. Epithelial Cell and Membrane Permeability to Protons. In Garner A, O'Brien P, eds. *Mechanisms of Injury, Protection and Repair of the Upper Gastrointestinal Tract.* Chichester: John Wiley & Sons Ltd. 175-85, 1991.

Ito S. Functional Gastric Morphology. In Johnson LR, ed. *Physiology of the Gastrointestinal Tract.* New York: Raven Press 1987.

Johnson LR, McCormack SA. Regulation of Gastrointestinal Mucosal Growth. In Johnson LR, ed. *Physiology of the Gastrointestinal Tract.* New York: Raven Press 611-41, 1994.

Juliano RL. Signal transduction by cell adhesion receptors and the cytoskeleton: functions of integrins, cadherins, selectins, and immunoglobulin-superfamily members. *Annual Review of Pharmacology & Toxicology* 42:283-323,2002.

Kaibuchi K, Kuroda S, Fukata M, Nakagawa M. Regulation of cadherin-mediated cell-cell adhesion by the Rho family GTPases. *Current Opinion in Cell Biology* 11:591-96,1999.

Kamynina E, Staub O. Concerted action of ENaC,Nedd4-2, and Sgk1 in transepithelial Na^+ transport. *American Journal of Physiology* 283:F377-F387,2002.

Kivilaakso E, Kiviluoto T. Intracellular pH in isolated Necturus antral mucosa in simulated ulcerogenic conditions. *Gastroenterology* 95:1198-205,1988.

Kiviluoto T, Paimela H, Mustonen H, Kivilaakso E. Intracellular pH in isolated Necturus antral mucosa exposed to luminal acid. *Gastroenterology* 98:901-8,1990.

Kottra G, Frömter E. Rapid determination of intraepithelial resistance barriers by alternating current spectroscopy. I. Experimental procedures. *Pflugers Archiv - European Journal of Physiology* 402:409-20,1984.

Kottra G, Frömter E. Rapid determination of intraepithelial resistance barriers by alternating current spectroscopy. II. Test of model circuits and quantification of results. *Pflugers Archiv - European Journal of Physiology* 402:421-32,1984.

Kottra G, Frömter E. Barium blocks cell membrane and tight junction conductances in Necturus gallbladder epithelium. Experiments with an extended impedance analysis technique. *Pflugers Archiv - European Journal of Physiology* 415:718-25,1990a.

Kottra G, Frömter E. Determination of paracellular shunt conductance in epithelia. *Methods in Enzymology* 191:4-27,1990b.

Lewis SA, de Moura JL. Incorporation of cytoplasmic vesicles into apical membrane of mammalian urinary bladder epithelium. *Nature* 297:685-88,1982.

Little MP, McCarthy CF, Mooney PA, Walters KM. The relationship between gastritis and the effect of bile salts on Na, K-ATPase in human gastric mucosa. *Journal of Physiology* 273:61P-2P,1977.

Lloyd KC, Debas HT. Peripheral Regulation of Gastric Acid Secretion. In Johnson LR, ed. *Physiology of the Gastrointestinal Tract.* New York: Raven Press 1185-226, 1994.

Miller TA, Kokoska ER, Smith GS, Banan A. Role of calcium homeostasis in gastric mucosal injury and protection. *Life Sci* 69:3091-102,2001.

Mitic LL, Van Itallie CM, Anderson JM. Molecular physiology and pathophysiology of tight junctions I. Tight junction structure and function: lessons from mutant animals and proteins. *American Journal of Physiology - Gastrointestinal & Liver Physiology* 279:G250-G254,2000.

Monson RR, MacMahon B. Peptic ulcer in Massachusetts physicians. *New England Journal of Medicine* 281:11-15,1969.

Mustonen H, Kiviluoto T, Kivilaakso E. Luminal acid increases apical cell membrane resistance in isolated Necturus antral mucosa. *Gastroenterology* 102:A130,1992.

Mutoh H, Hiraishi H, Ota S, Ivey KJ, Terano A, Sugimoto T. Role of oxygen radicals in ethanol-induced damage to cultured gastric mucosal cells. *Am J Physiol* 258:G603-G609,1990.

Nagel W, Garcia-Diaz JF, Essig A. Contribution of junctional conductance to the cellular voltage- divider ratio in frog skins. *Pflugers Archiv - European Journal of Physiology* 399:336-41,1983.

Neher E, Sakmann B. Single-channel currents recorded from membrane of denervated frog muscle fibres. *Nature* 260:799-802,1976.

Palmer LG. Ion selectivity of the apical membrane Na channel in the toad urinary bladder. *J Membr Biol* 67:91-98,1982.

Paul DL. New functions for gap junctions. *Current Opinion in Cell Biology* 7:665-72,1995.

Podolsky DK. Peptide Growth Factors in the Gastrointestinal Tract. In Johnson LR, ed. *Physiology of the Gastrointestinal Tract.* New York: Raven Press 129-67, 1994.

Puceat M. pHi regulatory ion transporters: an update on structure, regulation and cell function. *Cellular & Molecular Life Sciences* 55:1216-29,1999.

Rahner C, Mitic LL, Anderson JM. Heterogeneity in expression and subcellular localization of claudins 2, 3, 4, and 5 in the rat liver, pancreas, and gut. *Gastroenterology* 120:411-22,2001.

Reuss L. Changes in cell volume measured with an electrophysiologic technique. *Proc Natl Acad Sci U S A* 82:6014-18,1985.

Reuss L, Finn AL. Passive electrical properties of toad urinary bladder epithelium. Intercellular electrical coupling and transepithelial cellular and shunt conductances. *Journal of General Physiology* 64:1-25,1974.

Rutten MJ, Delcore R, Soybel DI, Moore CD, Cheung LY. Effects of cations and pH on apical membrane potential of in vitro Necturus antrum. *Am J Physiol* 256:G798-807,1989.

Rutten MJ, Moore CD. Low doses of ethanol have Ca2+ ionophore-like effects on apical membrane potential of in vitro Necturus antrum. *Am J Physiol* 261:G92-103,1991.

Sachs G. The Gastric H,K ATPase Regulation and Structure/Function of the Acid Pump of the Stomach. In Johnson LR, ed. *Physiology of the Gastrointestinal Tract.* New York: Raven Press 1119-38, 1994.

Seber GAF, Wild CJ. Statistical Interference. *Nonlinear Regression.* New York: John Wiley & Sons 191-270, 1988.

Shiba H. Heaviside's "Bessel cable" as an electric model for flat simple epithelial cells with low resistive junctional membranes. *J Theor Biol* 30:59-68,1971.

Siegenbeek van Heukelom J, Denier van Gon JJ, Prop FJA. Model Approaches for Evaluation of Cell Coupling in Monolayers. *J Membr Biol* 88-110,1972.

Singer MV. [What control solutions should be used in studies on the acute effect of alcohol on the gastrointestinal tract?]. *Z Gastroenterol* 21:567-73,1983.

Sprong H, van der SP, van Meer G. How proteins move lipids and lipids move proteins. [erratum appears in Nat Rev Mol Cell Biol 2001 Sep;2(9):698.]. *Nature Reviews Molecular Cell Biology* 2:504-13,2001.

Stein W. *Transport and Diffusion Across Cell Membranes*. San Diego: Academic Press, 1987.

Stryer L. *Biochemistry*, 4th ed. New York: Freeman co., 1995.

Sue MW, Guth PH. A fluorescent in vivo microscopic method to assess surface mucosal integrity in the rat stomach. Effects of ethanol and prostaglandin. *Gastroenterology* 89:415-20,1985.

Taylor JR. *An Introduction to Error Analysis*. Mill Valley: University Science Books, 1982.

Tepperman BL, Jacobson ED. Circulatory Factors in Gastric Mucosal Defence and Repair. In Johnson LR, ed. *Physiology of the Gastrointestinal Tract.* New York: Raven Press 1331-51, 1994.

Tsukita S, Furuse M, Itoh M. Structural and signalling molecules come together at tight junctions. *Current Opinion in Cell Biology* 11:628-33,1999.

Vasioukhin V, Fuchs E. Actin dynamics and cell-cell adhesion in epithelia. *Current Opinion in Cell Biology* 13:76-84,2001.